Impact of Planetary Siblings on Terrestrial World Measurements
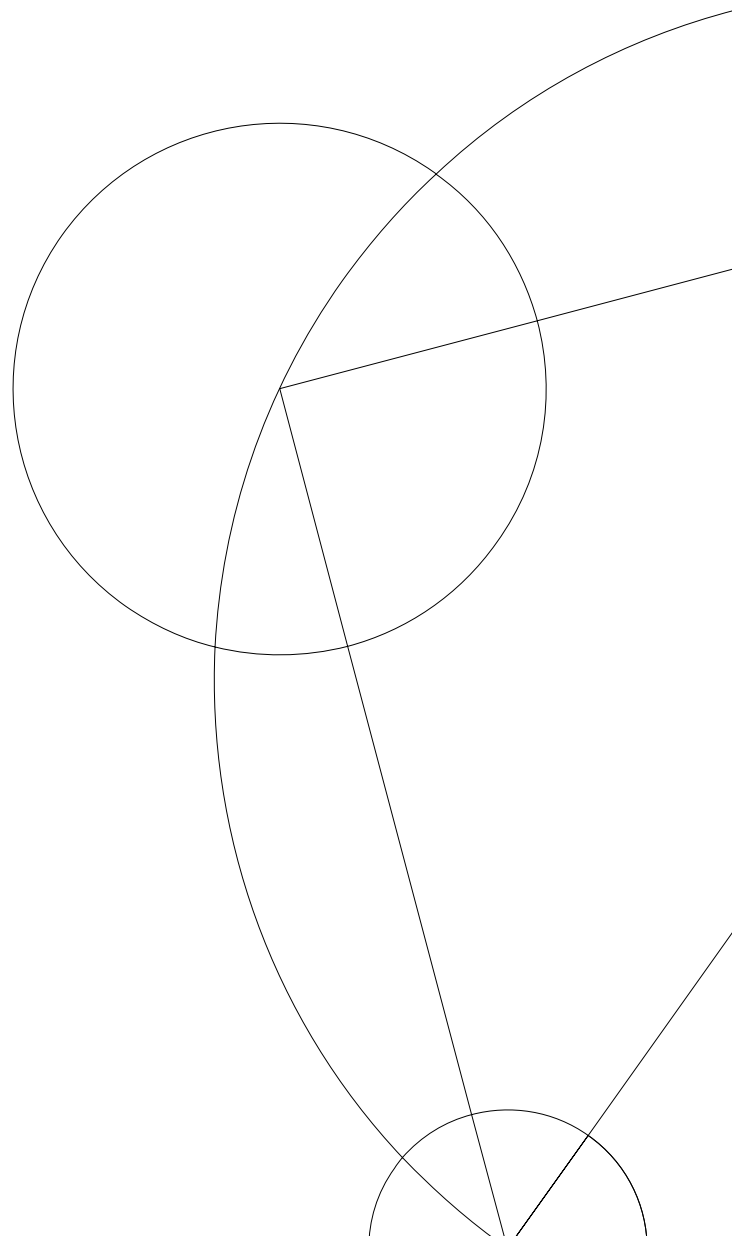
Masters Thesis

Written by:

Mette Baungaard, KU-id: ntq103

Advisor(s):

Prof. Lars Buchhave & Dr. Hannah Diamond-Lowe

FACULTY: Natur- og biovidenskabelige Fakultet

DEPARTMENT: Niels Bohr Institute

AUTHOR(S): Mette Baungaard

EMAIL: ntq103@alumni.ku.dk

TITLE: Impact of Planetary Siblings on Terrestrial World Measurements

SUPERVISOR(S): Professor Lars Buchhave & Dr. Hannah Diamond-Lowe

HANDED IN: 22.05.23

DEFENDED: 16.06.23

IN COLLABORATION WITH: DTU Space

NAME _____

SIGNATURE _____

DATE _____

Abstract

Small planets are abundant in our stellar neighborhood and commonly orbit around M-dwarf stars. These stars make up 75% of our stellar neighborhood, and with the era of James Webb Space Telescope (JWST) at our doorsteps, it is possible to characterize terrestrial exoplanets around these stars. This thesis investigates whether a planetary sibling can induce a measurable effect on the signal of a target planet observed in occultation. This thesis focuses on the exoplanet system LTT 1445A, a system of two planets orbiting an M-dwarf star. This system was chosen due to the proximity of the system to the solar system, as well as the host star being an M-dwarf, which is a cooler, smaller star and will make the signal the largest. I simulate the system using the code package `starry` and use the most up-to-date values for the parameters of the host star and planets. I make the simulated data in six different JWST MIRI instrument filters to see how the observational bandpass alters the observed signal. I set up the system and make simulated data and models for different planetary configurations, such as the planets containing atmospheres and situations where they do not. When defining the planets I take the extreme cases, where the incoming stellar radiation is entirely re-radiated from the sub-stellar point, creating a permanent hot spot for the no atmosphere case. For the atmosphere case, the atmosphere totally redistributes the incoming stellar radiation around the planet. I make a statistical analysis of the simulated data against a one-planet model to test if the presence of the sibling planet has a significant impact on the observations.

My results show that the presence of the sibling planet has a variably significant impact on the simulated light curve depending on the orbital phase of the sibling planet, as well as its semi-major axis. There is positive evidence of significance when the sibling planet is at phases 0.3 and 0.7 for specific filters. The impact of the sibling planet increases if it is moved closer to the star. The results indicate that certain situations are significant, and one can with confidence distinguish that there is a secondary planet with no atmosphere. This is exciting as in the era of JWST, there are programs to explore these multi-planetary systems around M-dwarfs, and with the results presented in this thesis, we are bound to characterize many more exoplanets.

Aknowledgements

Table of Contents

1 Introduction

The What

Understanding the signal we receive when observing celestial objects is integral to being an astronomer. There are many exciting fields within astronomy, and one that has received much attention in recent years is exoplanet research. Exoplanets are planets that orbit stars other than the Sun and are not part of the Solar System. There are many ways in which astronomers find and study exoplanets, such as the transit method, the radial velocity method, and the microlensing method, to name a few. This project focuses on the transit method, where astronomers detect planets that pass in front of their host star, between the star and the observer. This is called a transiting exoplanet. The result of such observations is a light curve, which shows the overall flux of the system as a function of time as the planet passes in front of the star. As the planet transits, the stellar flux dims, as the planet is covering some portion of the star. Figure 1 shows such a transiting planet and its projected light curve as it moves around the star in its orbit.
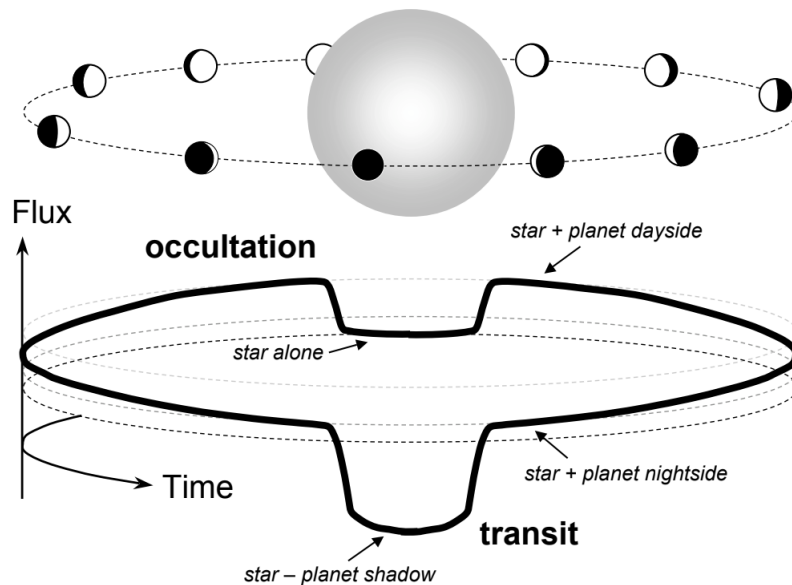
Figure 1: Illustration of planet trajectory around a star at each phase and the corresponding flux progression. Only the combined flux of the system is observed. We see that as the planet transits, the flux dips; this is due to the planet blocking a portion of the stellar flux. As the planet moves towards occultation, the planet's dayside comes into view and contributes to an increase in flux. The flux drops once again as the planet occults, though not as much as during the transit. Figure from Winn (2010).

Opposite the transit, a planet can also have an occultation (sometimes referred to as a secondary eclipse). An occultation is when the planet moves behind the star, and the star completely blocks its light. As Figure 1 shows, the planet begins to turn its so-called dayside toward the observer as the planet moves towards occultation. In Figure 1, we see that the

planet's dayside receives and then reflects or absorbs the stellar light, contributing flux to the overall light curve of the whole system before and after the occultation event.

When looking for exoplanets, the system's configuration is essential and can drastically change the probability of finding planets. Looking for planets with short periods, meaning they revolve around the host star quickly, gives much better results in finding planets, this can be seen in the transit probability equation, which states:

$$p = R_\star/d \tag{1}$$

Where p is the probability of a transiting exoplanet, and this equation depends on the stellar radius, $R_\star$, and the planet's semi-major axis, d. From this equation, it is clear to see that the smaller the semi-major axis, the higher probability of a transiting exoplanet (Seager & Lissauer, 2010). Short-period planets are hotter, and observing such planets requires relatively little telescope time as they move quickly in front of the star. As a result, astronomers have discovered numerous short-period planets which are likely tidally locked. Tidal locking refers to the phenomenon where one side of the planet constantly faces the star. Tidally locked planets can appear as a so-called "eyeball" planet, as the planet has a hot spot on the dayside part of the planet and a much cooler night-side. Figure 2 shows an eyeball planet, LHS 3844b (Kreidberg et al., 2019).
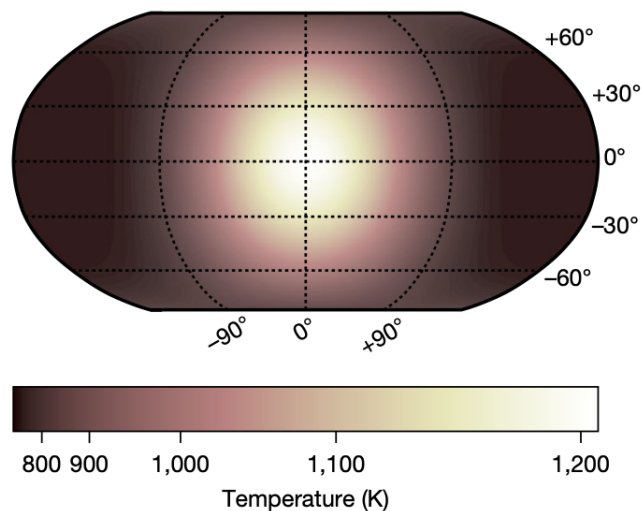
Figure 2: The following figure displays the surface map of planet LHS 3844b. We can see that the hot spot has a significantly larger temperature than the night side of the planet, creating this eyeball planet look. Figure from Kreidberg et al. (2019).

Whether small exoplanets orbiting M dwarfs have atmospheres is still unknown, which is a big question the research field is trying to solve. The extra light from the planet's dayside during these secondary eclipses can serve as a potential tool for atmospheric exploration, allowing us to probe the atmospheric presence, and possibly even composition. Depending on if

the planet has or does not have an atmosphere, this extra amount of flux from the planet will change. A thick atmosphere can redistribute stellar radiation and transfer the radiation from the dayside to the night-side, in the extreme case resulting in a complete redistribution of stellar radiation around the planet. Before the launch of the James Webb Space Telescope (JWST), measuring flux from a planet's dayside was limited as this method relies on observing in the mid- to far-infrared wavelengths, which many telescopes before JWST were not capable of.

The Why

When observing planets far beyond the Solar System, it is challenging to characterize the properties of the planets, such as their masses, radii, and atmospheric compositions. Astronomers observe planetary systems and decode the received signal to understand the information it holds about what they see. This task is challenging, as many factors affect the received signal and can drastically change the results. When observing planetary systems, astronomers must consider various effects, including those arising from the telescope, astrophysical phenomena, and possibly any unknown hidden planets. This project delves into the last one as a variable that can affect the signal.

An outstanding question in exoplanet research is whether or not certain exoplanets have atmospheres. Some planets are more accessible to characterize due to the system's configuration. Particular configurations are most favorable for atmospheric investigation, such as the system's proximity to us and the distance between the planet and the star. If the system is closer to the observer, the precision of the data is much better; if the planet is closer to its host star, the effect of the stellar radiation on the planet is more noticeable. Some planets are more challenging due to disturbing factors that affect the signals. One such factor is other planets that are orbiting close to each other. When observing a planet in such a configuration, where it is close to another planet, astronomers need to consider how much this other planet can affect the overall signal. Using simulated data, I look at a system with two planets with close orbits to their host star. Depending on the type of planet and whether or not they have atmospheres, I research if differing situations are noticeable in the signal received from the system. If this is a noticeable effect, this could be another method to determine if there are additional planets and if they have atmospheres. This is the project's main scope: to determine if a secondary planet induces a noticeable effect by simulating JWST data of a multi-planet system.

This project works specifically with simulated data from JWST due to the ability of the telescope to detect thermal emission from planets at infrared wavelengths. Figure 3 shows the different wavelength bands different telescopes operate at; note that specific molecules are detectable only in JWST's wavelengths. This research is significant as the findings could indicate that characterizing exoplanet atmospheres could be simplified or that additional methods are
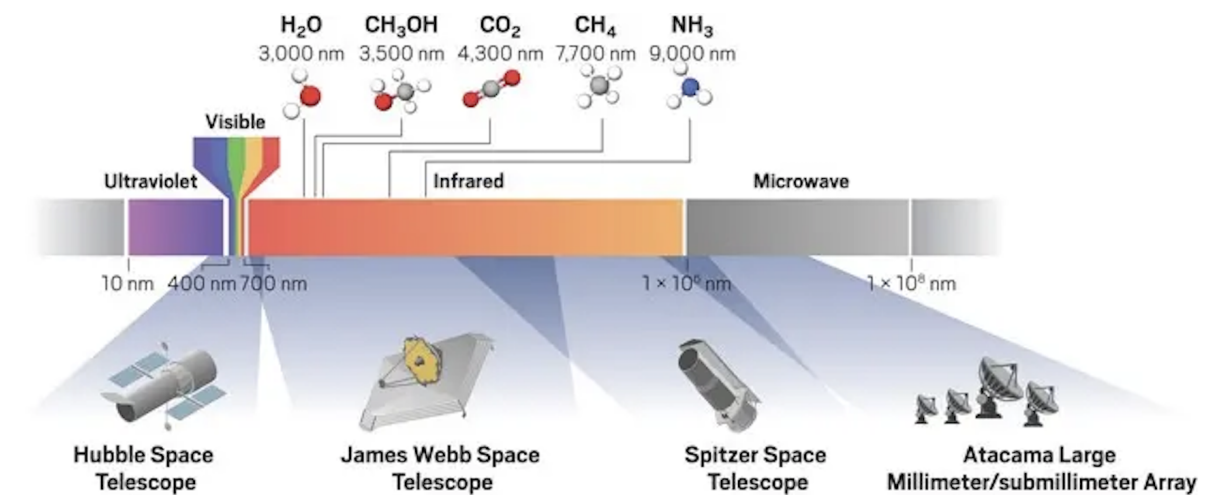
Figure 3: An illustration of the electromagnetic spectrum and where some telescopes observe. There can be seen to be some overlapping of the different telescopes. JWST is the telescope that observes most of the IR spectrum and also the wavelengths that contain spectral features. Credit: cen.acs.org/

required to confirm their presence, as the received signals alone are inconclusive. Exoplanet research is a core science theme of the JWST mission.

1.1 The History

The research field of exoplanets is relatively young. Starting in the 1980s, astronomers observed the first planetary disk, Beta Pictoris (Smith & Terrile, 1984). A protoplanetary disk is the birthplace of planets. It is a disk of material, mainly composed of gas and dust, that surrounds the young star and forms all types of planets over time, from rocky to gaseous. In 1989 astronomers revealed an exciting discovery: the first possible exoplanet. Although it was not confirmed, David W. Latham and his colleagues proposed the possibility of an exoplanet around a sun-like star due to finding periodicity in the star's motion (Latham et al., 1989). In 1990, the famed Hubble Space Telescope (HST) launched, which sparked a new era of astronomy. HST's scientific mission was to investigate the universe in visible, ultraviolet, and near-infrared wavelengths. It was mainly used to explore other stars, distant galaxies, and the planets in our solar system. However, it became a powerful tool for achieving atmospheric follow-up measurements of exoplanets (e.g., Charbonneau et al., 2002; Deming et al., 2013; Kreidberg et al., 2014; Sing et al., 2016). In 1992, the first official exoplanet discovery came. Aleksander Wolszczan and Dale Frail announced the discovery of two rocky planets orbiting a pulsar (Wolszczan & Frail, 1992). A pulsar is a rapidly rotating neutron star (the remnant of a giant dead star) emitting an insufferable amount of radiation. A problem with this discovery is that this system is very far away, with a distance of around 705 parsecs from the solar system, making it difficult to study the atmospheres of these worlds, if they have any.

In 1995 the first confirmed exoplanet to orbit a solar-type star was discovered. Mayor & Queloz (1995) discovered a Jupiter-mass companion to the solar-type star 51 Pegasi. This discovery opened up the whole field of exoplanet research and was awarded the Nobel Prize in Physics in 2019. The first transiting exoplanet was discovered in 1999, presented by Charbonneau et al. (2000). At the start of the 21st century, in the 2000s, exoplanet research starts taking great leaps. In 2001 alone, two very influential discoveries were announced, one of which was the discovery of an exoplanet within the habitable zone (NASA Historic Timeline, 2022). This is a zone around a star where the region's temperatures support liquid water; thus, planets in these regions can possess water. Water is a crucial ingredient for life as we know it on Earth. The other discovery is the first measured atmosphere of an exoplanet (Brown et al., 2001).

Since the launch of HST, astronomers have launched many telescopes, including the Spitzer Space Telescope and the Kepler Space Telescope. Although Spitzer was not initially launched with the intention of studying exoplanets, innovations during its mission enabled it to detect planetary transits and eclipses, as well as provide atmospheric constraints in the infrared. Interestingly, as Spitzer could detect secondary eclipses in the IR, it could detect direct light from the planet. When Spitzer was launched in 2003, astronomers did not know how common exoplanets were. When the Kepler Space Telescope launched in 2009, it played a significant role in eventually revealing how common exoplanets are. Its primary science mission was to explore planetary systems' prevalence and diversity [1]. Kepler's observing strategy consisted of observing the same patch of space for four years, showing that exoplanets are common, specifically small ones (Borucki et al., 2010). Another notable telescope is ESA's CoRoT space telescope; it launched in 2006 with the primary mission to detect exoplanets, specifically transiting exoplanets, and explore the physics of stars [2]. CoRoT was Europe's first telescope launched with this purpose.

In the 2010s, finding new exoplanets booms, with the help of the new technology made to look for these planets. In 2018 another exoplanet-research telescope, TESS, was launched. Compared to Kepler, TESS is not as static but covers most of the sky and specifically looks for the closest exoplanets around the brightest stars. These findings are more promising for follow-up investigations to determine the planets' masses and possibly even to study their atmospheres [3]. Since the launch of HST, astronomers have discovered countless exoplanets and probed many atmospheres.

We are currently in the 2020s, a decade filled with excitement. Up until submitting this

---

[1] NASA Mission Page Kepler Overview
[2] CoRoT ESA Overview
[3] NASA TESS Overview

thesis, researchers have discovered over 5000 exoplanets (NASA Exoplanet Archive, 2023). In December 2021, the James Webb Space Telescope (JWST) finally launched, initiating its mission to provide the most detailed observations of exoplanet atmospheres to date. Additional theme goals of JWST are; the assembly of galaxies, by observing the earliest galaxies, as well as the birth of stars and protoplanetary disks [4]. We can anticipate numerous thrilling discoveries in the coming decade and beyond.

Breakdown of Thesis

This thesis explores the influence of sibling planets on secondary eclipse observations of a target planet, by harnessing the capabilities of the most advanced telescope in our era for terrestrial exoplanet discovery. Trying to get the most out of a given secondary eclipse observation, I aim to determine whether the unseen influence of a sibling planet on a light curve can provide insights into the atmospheric conditions of the sibling itself. A complete setup of a test system (LTT 1445A, see section 1.6.1 for further information) starts the analysis, and I can probe this problem with different tests. I will test the position of the planets in their orbit relative to each other and the orbital distances of the planets around the host star by changing the semi-major axis and thus changing the planet's temperature. First, I will highlight the necessary theory needed to understand the physics in the thesis; then, I will introduce my methodology, how the code is set up, which parameters I chose, and why. Lastly, I will present my results and discussion, including diving into further applications of the results and my thesis.

1.2   Detection of Exoplanets

Several methods are available to detect exoplanets, and each method reveals different properties, such as mass, radius, orbital period, distance from the stellar host, etc. A few of these methods include radial velocity, direct imaging, transits, and microlensing. The following section will briefly explore the different exoplanet detection methods, explaining their workings and the properties deduced from each method.

1.2.1   Radial Velocity

The radial velocity (RV) method was used to detect the first exoplanets around sun-like stars and is an integral part of the exoplanet discovery story. This method builds upon the Doppler effect, theorized by Christian Doppler in 1842. If an observer moves with respect to

---

[4]STScI James Webb Science Goals

the emitter, a photon emitted at a specific wavelength in the rest frame of the emitter will be measured to have a different wavelength in the frame of the observer. This can be as an increase or a decrease in wavelength, depending on if the observer's movement is to or from the emitter. In the context of the RV method, this indicates that if planets orbit around stars, they pull on the star slightly, making it wobble, which is detectable using the Doppler method (Lovis & Fischer, 2010). Astronomers then observe systems and see if the stellar spectral lines have shifted over time. The presence of atoms or molecules causes the absorption or emission of light, leading to the creation of these spectral lines. If there is a shift in the spectral lines, the separation can give insight into the star's radial velocity and wobble. Using the Doppler effect, it is possible to track the velocity of the star as it wobbles due to the planet pulling on it, and over time this creates a periodic curve, see Figure 4.
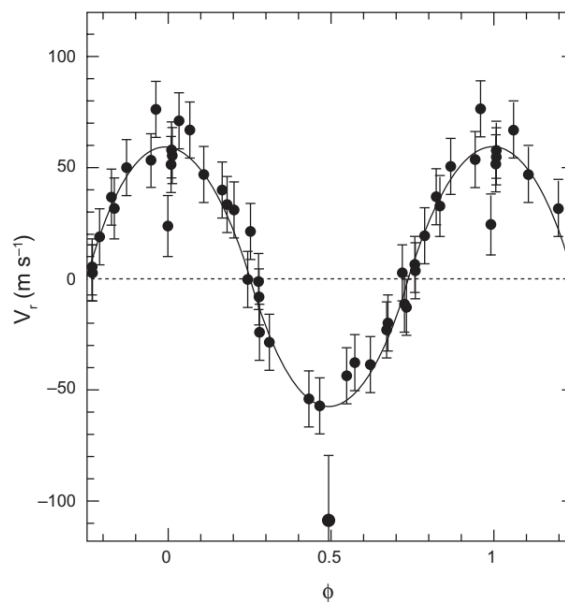

Figure 4: RV curve for the star 51 Pegasi observed with the ELODIE spectrograph at the Haute-Provence Observatory of France. This curvature observed in the signal is due to an orbiting planet. This finding revealed for the first time an exoplanet around a solar-type star. Figure from Mayor & Queloz (1995).

The period of this sinusoid is the period of the planet's orbit around the host star, this can be used to calculate the distance at which the planet orbits by using Kepler's third law. With the planet's orbiting distance, we can calculate the velocity of the planet, and furthermore, a minimum mass of the planet, as the orbital inclination of the planet is not always known. Note this minimum mass of the planet is relative to the stellar mass; in order to get just the planetary mass, one would need to know the stellar mass, as well as the planet's orbital inclination. The mass, distance from the star, and period are the main properties of exoplanets that can be found using the RV method.

The RV method was the most used method of detecting exoplanets for many years and

can calculate several properties beneficial to characterizing exoplanets. RV works best for more massive planets, such as hot Jupiter-sized planets, as these will have a more considerable gravitational pull on the star than a much smaller planet like the Earth, which will pull much less. Furthermore, RV also works well if the planets have a closer orbit to their host stars. A disadvantage to this method is that the system's configuration must be as edge-on as possible, meaning the system's plane is toward the observer. If the plane is not oriented towards the observer and remains perpendicular, it becomes impossible to detect the radial velocity, rendering the method unusable. However, if the planet undergoes a transit, it provides a precise constraint on the inclination, leading to improved mass calculations.

1.2.2   Transits

When the system's plane is edge-on, one can use the RV method or take advantage of planetary transits and occultations. As described, transiting planets cross in front of their host stars as seen from the observer's perspective. When the planet moves behind the star, we have an occultation; the star completely blocks the planet as it moves behind (see Figure 1). When astronomers look at the collected light of the system, many properties can be deduced, much more than with the RV method alone. The main properties one can deduce from the light curve are the radius and period. The period we can find due to needing multiple transits to confirm the planets. With the transit method, the radius is found as a planet-to-star ratio, defined as $k = \frac{R_p}{R_\star}$. The transit method and the RV method together become a powerful tool, where it becomes possible to measure the planet's bulk density, and surface gravity, as well as constrain stellar density (Lovis & Fischer, 2010).

Planets rarely have a sharp edge to their surface, for example, gas giants have no well-defined surface, and even rocky planets could possess a very thick atmosphere. This results in the absorption of some of the stellar light as the planets transit, as the starlight travels through the upper parts of the planetary atmospheres to our telescopes. This absorption is wavelength dependent on what atoms are present in the planet's atmosphere. When observing at a wavelength where strong atomic or molecular transitions occur, the atmosphere becomes more opaque, and thus the planet's silhouette is larger. This raises the possibility of learning more about the composition of the planet's atmosphere by observing a transmission spectrum (Winn, 2010).

1.3 Planetary Characterization

1.3.1 Spectroscopy

Spectroscopy is a method used to gain knowledge from light from celestial bodies by splitting the received light into each of its wavelength components, producing a spectrum. Spectra contain certain features, such as emission and absorption lines, produced by molecules and atoms. This means that the spectrum is not smooth but peppered with lines from the molecules' absorption and emission of light. Emission lines form when the light interacts with the molecules and causes them to get excited and thus emit radiation when returning to a lower excitation level. Absorption lines come from the absorption of radiation when interacting with molecules. These lines form at specific wavelengths and can thus be used to determine the atmospheric composition about the object observed (Carroll & Ostlie, 2017). One can, for example, use spectroscopy to calculate the redshift of galaxies by measuring how shifted the absorption or emission lines of specific known molecules are and comparing them to the known wavelength these lines should occur at. One could dissect the spectrum and observe if any lines from sought-after molecules or atoms are present. In the context of looking at exoplanets, this is a powerful tool to probe the possible atmospheres of exoplanets.

The most common type of planets are small terrestrial planets (Dressing & Charbonneau, 2013, 2015). The vast majority of the small planets detected, have short orbital periods, meaning they orbit closer to the host star, this is due to the observational biases of the transit and RV methods used to detect these planets. Dressing & Charbonneau (2013) research takes into account this detection bias, and thus the results are conclusive, small terrestrial planets are most common. The high probability of the planets being tidally locked and their proximity to the host star increases the uncertainty regarding their potential to possess atmospheres and exposes the possibility of hostile environments. There has yet to be a definitive observation of an atmosphere on a terrestrial planet, although recently, in May of this year, a new paper was published with the results of a possible detection of a thick water atmosphere around the exoplanet GJ 486b (Moran et al., 2023). Moran et al. (2023) present results that show that GJ 486b either has a thick water atmosphere due to the model of such an atmosphere agreeing quite well with the observations, or the observed signal is actually from contamination by the host star due to possible water vapor in cool starspots. Further observations are needed to disclose if this observation is indeed the first detection of an atmosphere of a terrestrial planet.

1.3.2 Thermal Emission

The primary method used in this thesis to investigate whether or not terrestrial planets have atmospheres is that of measuring planetary thermal emission. This method looks at the planetary thermal phase curves throughout the planet's orbit. It was first introduced by Seager & Deming (2009), who proposed a new technique to distinguish if tidally locked close-in orbit planets could harbor atmospheres. The idea of the method is to observe the signature of an atmosphere's redistribution of radiation or the lack thereof. A planet with a thick atmosphere will have a specific signature in its thermal phase curve due to the redistribution of the stellar radiation throughout the atmosphere. Contrary, if a planet is a bare rock with no significant atmosphere, it will produce a signature with a clear night-side and day-side difference in the signal (Koll et al., 2019). This method requires the observations to be done in the infrared wavelengths, and the JWST's MIRI instrument is an ideal tool to use with this method.

Previous investigations have been done using this method, such as for the planet LHS 3844b, investigated by Laura Kreidberg. Kreidberg et al. (2019) found this planet to have a very hot day-side temperature and a very low night-side temperature, thus resulting in a significant difference in the thermal phase curve, see Figure 5. As this planet is very hot and highly irradiated, the results of this paper highly motivate a similar investigation with cooler, less-irradiated planets.
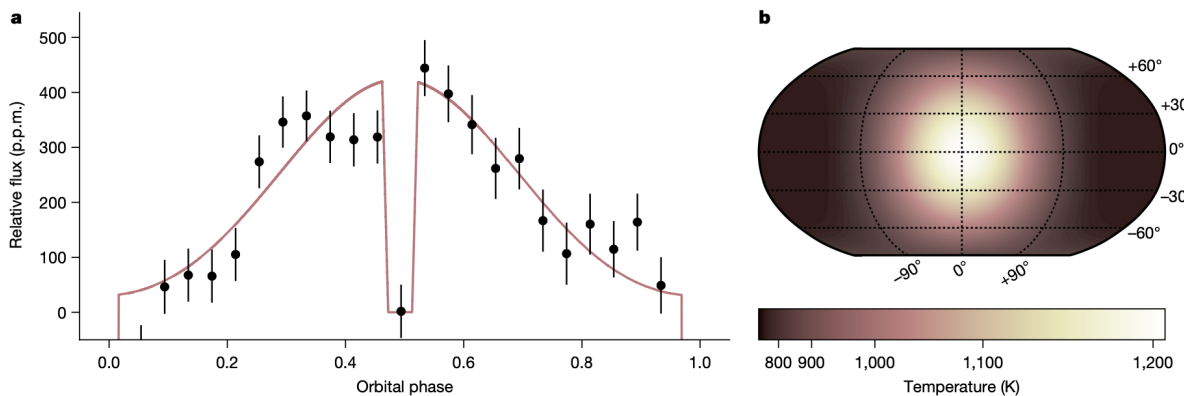

Figure 5: **a)** Planet-to-star flux ratio as a function of orbital phase, normalized to the star such. When the planet is at occultation at orbital phase 0.5, the flux is consistent with 0. The black points are the data, and the red is the best-fit line for the data. **b)** The spherical harmonic thermal map of the planet, indicating this clear eyeball planet characteristic. Figure from Kreidberg et al. (2019).

Although this method sounds promising in theory, it is also costly to distinguish and characterize planetary atmospheres. This is due to the long observing time needed to get the full phase curve; for example, to get the light curve of LHS 3844b, Kreidberg et al. (2019) observed for over 100 hours using Spitzer. Therefore, using eclipse photometry instead, where one takes multiple observations of secondary eclipses is much more time effective. This is due

to a secondary eclipse taking mere hours, and thus astronomers are able to make multiple observations in a much shorter time rather than taking a full phase curve observation (Koll et al., 2019).

1.4 M-Dwarfs

There are many types of stars in the Milky Way, and most stars can host planets. When looking for exoplanets, specific criteria for stars aid in the search for exoplanets. The first criterion is that the stars must be nearby to diminish the effect of the inverse square law, which states that the further away an object is, the more spread out the light emitted from the star is. Thus the apparent brightness becomes fainter with the square of the distance. The second criterion probes the stellar mass and radius; the planet-to-star ratio should be maximized. With the plethora of stellar types, one class of stars meets the criteria extraordinarily, namely M-dwarfs. These stars are abundant in the stellar neighborhood, making up approximately 75% of the stars closest to us (Segura et al., 2005). The closest M-dwarf star that hosts transiting exoplanets is LTT 1445A, at a distance of 6.86 pc (Winters et al., 2022). M-dwarf systems are believed to host mostly terrestrial planets and do not host many gas giants due to the lower stellar masses and, thus, slower formation timescales, indicating gas giants would not have time to form in such systems. Despite this, TESS has discovered a few transiting gas giants around M-dwarfs (Segura et al., 2005; Kanodia et al., 2023).

1.5 James Webb Space Telescope

The James Webb Space Telescope (JWST) has been in the works for decades now. In 1995 the Space Telescope Science Institute (STScI) proposed building a large telescope capable of observing infrared light. The telescope's construction started in 2004, and by 2011 the construction of the mirrors was completed [5]. JWST is a state-of-the-art telescope, as it is the first of its kind to be so large that to get it to space, a unique new technique to fold the telescope was introduced.

Design

When JWST is fully deployed, as shown in Figure 6, we can see many telescope parts. The telescope consists of the primary mirror, which includes 18 hexagonal mirrors that work together to become the primary mirror (Rauscher & Ressler, 2005). This specific design was developed concerning the telescope being foldable in order to fit inside Ariane 5, the rocket

---
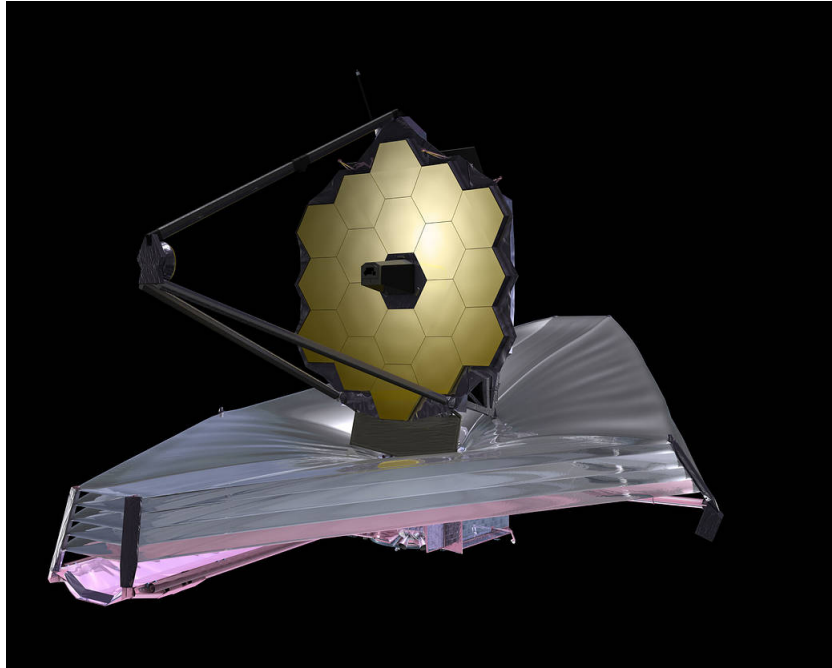
[5]JWST Mission Timeline website

Figure 6: Digital representation of the James Webb Space Telescope fully deployed. Credit: NASA.gov

bringing it to space. In addition to the primary mirror, there is the secondary mirror located at the tip of the structure. Crucial to JWST is the sun shield. For the telescope to not overheat, a unique sun shield is needed to keep the telescope at the right temperature. Furthermore, a sun shield is needed, as if the telescope is hot, it will add its own thermal signal to observations. This means the JWST has a warm sun-facing side and a much cooler space-facing side. This sun shield also needed the capability to fold and unfold perfectly.

Instruments

JWST is fitted with an array of instruments with different capabilities. These instruments are the Fine Guidance Sensor (FGS), the Near-Infra-Red Camera (NIRCam), the Near-Infra-red Spectrograph (NIRSpec), the Near-Infra-Red Imager and Slitless Spectrograph (NIRISS), and lastly, the Mid-Infra-Red Instrument (MIRI). The FGS is used to ensure that a guide star is available at any point in the sky, with >95% probability (Rauscher & Ressler, 2005). NIR-Cam is an instrument that is suited for the observations of early galaxies. It observes in the wavelength band of 0.6 to 5.0 microns. It offers different observing modes, such as imaging, coronagraphy, wide-field slitless spectroscopy, time-series imaging, and grism time series. The wavelength band is further separated into a long and short wavelength band, where the short wavelength band covers 0.6 to 2.3 μm, and the long wavelength band covers 2.4 to 5.0 μm (JWST User Documentation, 2016). NIRSpec is, as the name implies, the instrument that provides near-IR spectroscopy in a wavelength band similar to NIRCam, of 0.6 to 5.3 μm. It can be used to measure redshift, the metallicity of stars, star formation, and characterization of exoplanet atmospheres using transit observations (JWST User Documentation, 2016). It has four

observing modes: Multi-object spectroscopy, imaging spectroscopy, high contrast single-object spectroscopy, and high throughput bright object time-series spectroscopy. NIRISS is an instrument that provides observing modes for slitless spectroscopy and imaging at wavelengths of 0.6 to 5 μm. NIRISS has an observing mode that is dedicated to exoplanet research named SOSS, which stands for Single Object Slitless Spectroscopy. This mode is ideal for time-series observations. Lastly, MIRI is an instrument capable of imaging and spectroscopy observing modes in wavelengths between 5 to 28 μm. This specific instrument is the focus instrument of JWST for this thesis. The following section will go into the details of MIRI.

MIRI

The MIRI instrument observes in the wavelengths 5 to 28 μm; this enables the instrument to be utilized in studies of direct imaging of warm exoplanets and probing their atmospheres using spectroscopy. Furthermore, MIRI also enables the identification and characterization of galaxies at redshift, z > 7, thus meaning these are some of the first galaxies in the universe. MIRI can achieve these studies by offering a broad range of observing modes. These modes include; imaging, low-resolution slitted and slitless spectroscopy, medium-resolution integral field unit (IFU) spectroscopy, and coronagraphy. [6]

The observing mode chosen for this thesis is the imaging mode as a time series. This mode is used for photometric observations, which build on the premise that the photons are collected into big "buckets" rather than spread out as in a spectrum. This enables the collection of more photons per integration and increases sensitivity, which is helpful when working with smaller signals. Furthermore, it allows the observation of much longer wavelengths. The MIRI imager provides nine broadband wavelength ranges to be observed, although one filter, F1130W, is narrower to isolate the 11.3 μm Polycyclic Aromatic Hydrocarbon (PAH) emission feature. These filters were designed to enable observations over the entire wavelength range, with few gaps in the wavelength coverage. Figure 7 shows the filter bandpasses.
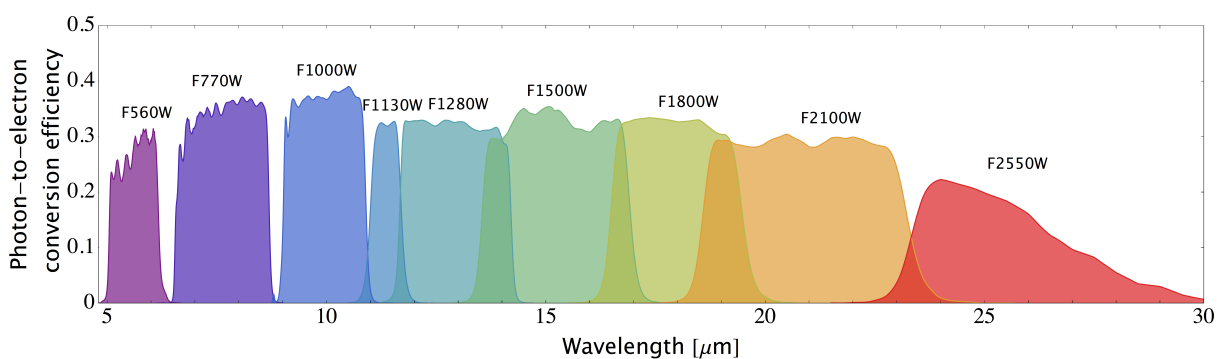

Figure 7: The nine filter bandpasses for the MIRI imaging mode. Credit: (JWST MIRI Documentation)

---

[6]JWST MIRI Docs

The filters chosen for this thesis are F1130W up to F2550W, giving six filters in total. The colors of the filters in Figure 7 will be conveniently used as the color code for the filters in the plots created for this thesis to ensure continuity throughout. In previous papers, such as Greene et al. (2023), the preferred filter used in observation is F1500W due to the filter coinciding with a strong CO_2 absorption feature.

1.6 Exoplanet Systems

1.6.1 LTT 1445A

The primary system investigated in this thesis is LTT 1445ABC. Located 6.86 pc away, it is a nearby triple M-dwarf system. Two of the stars, LTT 1445B and LTT 1445C, are a tight binary pair, and together they orbit around a common center of mass with LTT 1445A (Winters et al., 2019). This project is specifically looking at LTT 1445A, which has been found to host transiting exoplanets. The first confirmed exoplanet in the system was discovered in 2019 using TESS data presented by Winters et al. (2019). This planet is LTT 1445Ab. A few years later, Winters et al. (2022) presented another planet, LTT 1445Ac. This second planet was discovered while taking radial-velocity measurements; a second periodic signal displaying transit-like characteristics was found in the TESS data. Using the RV measurements, the TESS data, and ground-based photometric monitoring, it was concluded that a second planet was transiting LTT 1445A. Furthermore, this new planet was found to orbit interior of the previously found planet LTT 1445Ab (Winters et al., 2022). This is an exciting system, as LTT 1445 A is the closest M-dwarf to host transiting exoplanets.

Both LTT 1445Ab and LTT 1445Ac are likely terrestrial planets, with LTT 1445Ab falling on the earth-like composition curve, as seen in Figure 8. Notably, LTT 1445Ac also falls on this curve in the figure. However, due to the planet's radius not being constrained and instead only being a lower limit, it can theoretically be of a different composition. This is due to the inclination measured from the observed light curve being consistent with a grazing transit (Winters et al., 2022). A grazing transit is one where not all of the planet transits in front of the host star. LTT 1445Ab has a radius of 1.305 Earth Radii and a mass of 2.87 Earth Masses; it has an orbital period of 5.3587 days (Winters et al., 2022). LTT 1445Ac has a radius of 1.147 Earth Radii and a mass of 1.54 Earth Masses, with an orbital period of 3.12 days (Winters et al., 2022).

Although much is not known yet about the characteristics of the planets, this system is a fantastic candidate to use JWST to probe its planets further. In JWST cycle 1, there is a program (GO 2708) to observe the thermal emission spectrum of LTT 1445Ab in secondary
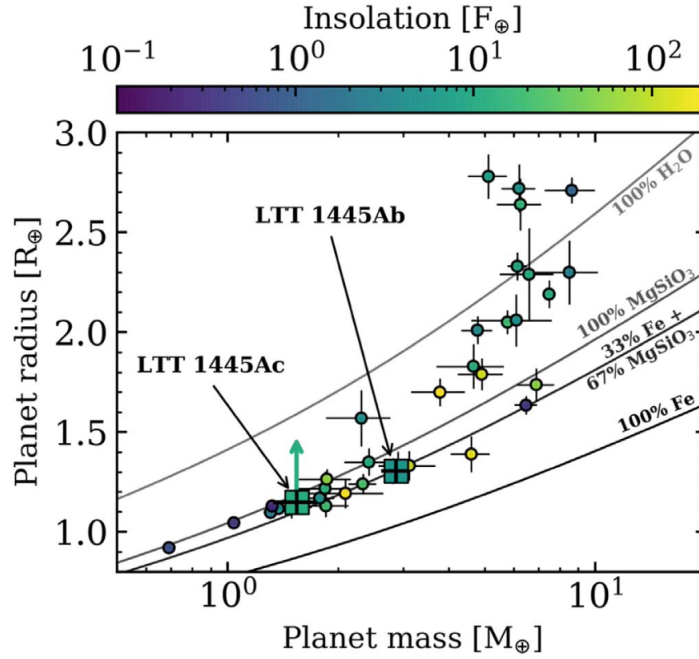
14

Figure 8: This figure shows the masses and radii of small planets transiting M-dwarfs. On the x-axis is the planetary mass in terms of Earth masses, and on the y-axis is the planetary radii in terms of Earth radii. The solid lines show different compositions of planetary interiors. LTT 1445Ab and LTT 1445Ac are shown with green squares. LTT 1445Ab falls on the composition that is Earth-like with 33% Iron and 67% rock, whereas LTT 1445Ac falls on the same composition line, but due to the radius of the planet not being constrained, it could be of a different composition. Figure from Winters et al. (2022).

eclipse to probe if it has an atmosphere (Berta-Thompson et al., 2021). Furthermore, choosing this system is beneficial, as the system is the most favorable due to being nearby, and thus making observations of it much better compared to a further away system.

2 Method

Throughout this project, I use the publicly available `starry` code, which enables users to efficiently compute light curves for celestial bodies and manipulate them in many ways.

2.1 Starry Python Package

`starry` is a code package that enables users to map stars and exoplanets (Luger et al., 2019). `starry` is a versatile tool where one can create exoplanet systems, explore the dynamics and properties of the system, or change certain system aspects to test new hypotheses [7].

Making a system in `starry` is straightforward; one starts with defining the host star and the planets. When defining the host star, the user defines a primary object. See the following

---

[7]Starry Webpage

example:

```
star = starry.Primary(starry.Map(ydeg=0, udeg=2, amp=1.0), m=1.0, r=1.0, prot=1.0).
```

The first argument when defining a primary object is to define the map. `starry.Map` creates the surface map of the object. A few different types of maps are available when defining the surface map of an object. These include spherical harmonic maps, limb darkening maps, radial velocity maps, and a few more. For this project, the spherical harmonic maps are the focus. The arguments in `starry.Map` include `ydeg`, `udeg`, and `amp`. The first argument, `ydeg`, refers to the spherical harmonic degrees; see Figure 9a. This argument can create almost any type of surface map, from entirely plain with no special features, to a replica of a cloudless Earth, as seen in Figure 9b. In the code example, notice that the `ydeg` = 0; this is the default and returns a uniform surface map with no special features.

(a) Spherical Harmonics up to a degree of l = 5.

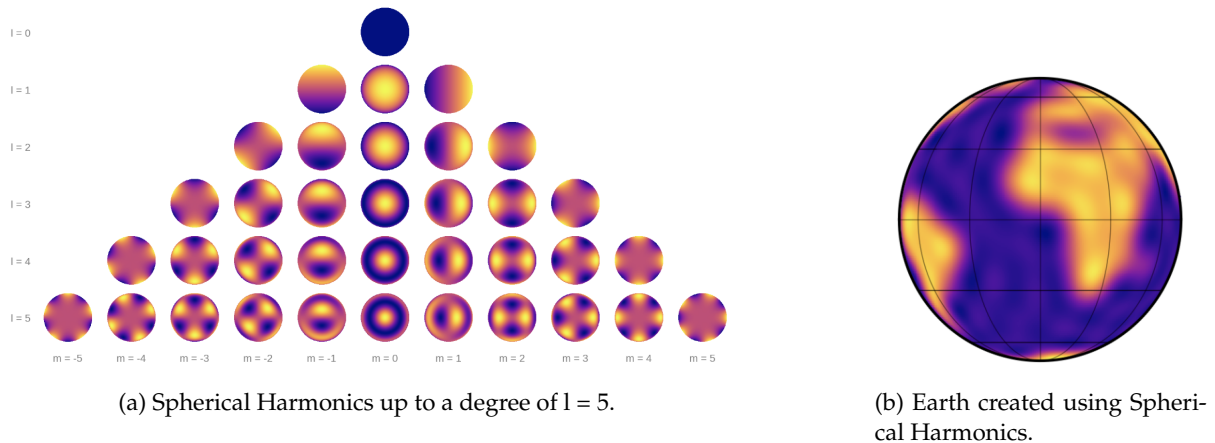(b) Earth created using Spherical Harmonics.

Figure 9: Spherical Harmonics examples from Luger et al. (2019)

The second argument, `udeg`, pertains to the degree of limb darkening filter. Limb darkening is a phenomenon that occurs in stars, where the central part of the star appears to be brighter than the edge, also known as the limb. This effect varies from star to star, according to which type of star it is, but this effect also differs when observing planet transits at different wavelengths. Limb darkening is not observable unless there is a planet transiting. Therefore this effect is essential when creating stellar bodies in `starry` but unnecessary when creating planetary objects.

The last argument when defining the map of the object is `amp`. This signifies the overall amplitude of the map and can be in arbitrary units. The rest of the stellar parameters are defined when the map has been defined. `starry` must have a mass, m, a radius, r, and a rotational period, prot. The mass and radius can be scaled to the stellar parameters. However, this means that the whole system, including possible secondary objects like planets, must be scaled to the stellar parameters.

16

The secondary orbiting objects are defined similarly; see the following code example:

```
planet = starry.kepler.Secondary(
    starry.Map(ydeg=5, amp=5e-3), # the surface map
    m = 0, # mass in solar masses
    r = 0.1, # radius in solar radii
    porb = 1.0, # orbital period in days
    prot = 1.0, # rotation period in days (synchronous)
    Omega = 0, # longitude of ascending node in degrees
    ecc = 0.3, # eccentricity
    w = 90, # longitude of pericenter in degrees
    t0 = 0, # time of transit in days
    theta0 = 180 # rotational phase of map at t0 in degrees)
```

It is defined using the `starry` class `Secondary`, and the map is defined similarly. Likewise to the primary object, one has to define the surface map. Particularly for planets, the surface map tends to be more complex, as terrestrial planets especially tend to contain unique surface or atmospheric features, such as oceans and clouds. In the example above, the map is more complex than the primary object example, as it has `ydeg` = 5. Specifically, `starry` is setting up the vector `y` to make the surface map of the object. This vector is defined as;

$$y = Y_{l,m} = \{Y_{0,0},\ Y_{1,-1},\ Y_{1,0},\ Y_{1,1},\ Y_{2,-2},\ Y_{2,-1},\ Y_{2,0},\ Y_{2,1},\ Y_{2,2},\ \ldots\ \}$$

Setting `ydeg` to 5 means that the degree is set to 5, the degree is `l`, and the mode, `m`, are the columns in Figure 9a. The mode goes from order `m` = -1 to `m` = 1. For the example with `ydeg` = 5, all the different degrees and modes in the 9a can be used to create the surface map. One can make detailed maps using increasing degrees and varying modes. The overall amplitude must also be defined; this is the same concept as for the primary object. Next, the mass, radius, orbital period, rotational period (`prot`), eccentricity (`ecc`), and transit time (`t0`) in days are defined. The longitude of the ascending node (`Omega`) and the longitude of pericenter (`w`) are used to specify where the planet is in orbit; this is not necessary for my project and has been kept at the default values, as seen in the example, due to my assumption that the planets have an eccentricity of 0. Lastly, one can also define `theta0`; this is the rotational phase of the map at `t0` in degrees. When I set up the system initially, I rendered a video of the system to visualize the setup more clearly. This was when I noticed that the "eyeball" I had created was facing the wrong way, meaning the hotspot faced away from the star, towards the observer at transit, which is not the proper setup. By turning the map with `theta0` = 180 degrees, I turned the hotspot around, towards the star, and away from the observer.

The time of transit parameter indicates at what time the center of the transit occurs. This can be written in terms of days but can also be written in terms of the orbital phase of the planet. To write in terms of the orbital phase, one takes the orbital phase needed and multiply by the orbital period. In starry, I noticed that the orbital phases seemed to be "reversed". The intuitive direction of the orbital phase progression goes from orbital phase 0 at transit and moves to orbital phase 0.25 at the quarter phase to occultation. At occultation, the orbital phase is 0.5, and so on. When defining the system and doing tests at the beginning of the project, I discovered that defining the time of transit parameter in terms of the orbital phase introduced a "reversed" orientation of the orbital phase progression. See Figure 10 for a diagram.
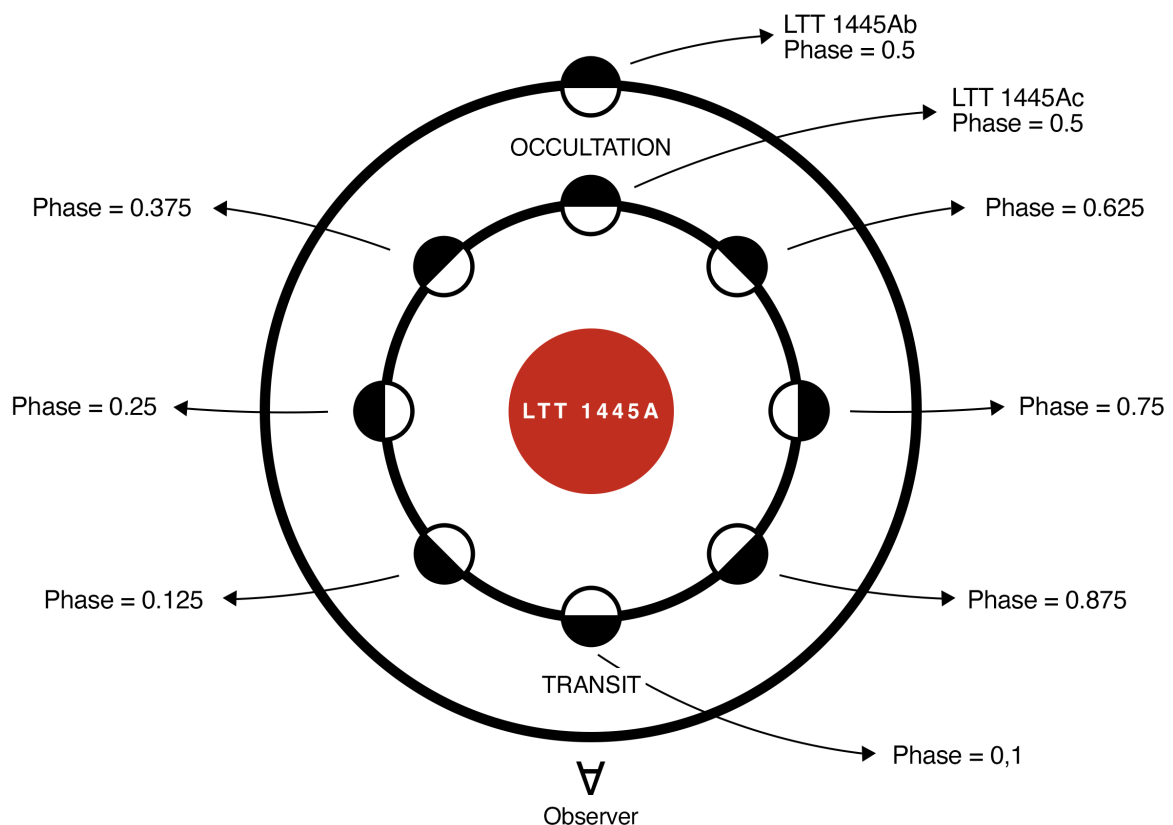

Figure 10: This diagram shows a bird's eye view of the LTT 1445A system. Showing LTT 1445Ab at occultation and LTT 1445Ac at different phases and the corresponding phase values in the code. Credit: Image created by Mette Baungaard and illustrated by Nikola Trajkovski.

As shown in Figure 10, the phase progression goes from 1 and moves "backward" towards 0 as the planet progresses through its orbit. Note this does not mean that the planets orbit clockwise but continue to move in the natural direction of counterclockwise. This progression is unusual, but this "reversed" nature has been considered after thorough tests and does not pose a problem to the analysis.

Once the planets and star are defined, the system can be easily set up using the function System = starry.System(star, planet1, planet2, ...). Here the first input in the func-

tion is the primary object, typically the star, and the input after are the secondary objects. When the system is created, the planets are positioned at time 0, at the center of the transit; this is defined by the transit time parameter, `t0` when defining the planets. One goal for the thesis is to investigate how the position of one planet, with respect to another, would change the signal received, and for this reason, the definition of `t0` is best in terms of phase. Specifically, the definition of `t0` for planet LTT 1445Ac should be linked to the phase of LTT 1445Ab. LTT 1445Ab was set to start in transit; thus, `t0 = 0`, whereas LTT 1445Ac's position should depend on LTT 1445Ab's occultation position. I found a way to define LTT 1445Ac's position such that when set in the phase position, it follows LTT 1445Ab's phases. If I define the transit time parameter t0 for LTT 1445Ac to be the following, `t0 = (porb,b * 0.5) + (porb,c * PHASE)`, I get LTT 1445Ac at the correct position that corresponds to what phase is set in the above equation. The equation starts by taking the orbital period of LTT 1445Ab and multiplying it by phase 0.5; this gives the days at which LTT 1445Ab is occulting. Then the orbital period of LTT 1445Ac multiplied by the wanted phase position is added, resulting in LTT 1445Ac being the phase position inserted in the equation. To test this, I created Figure 11.
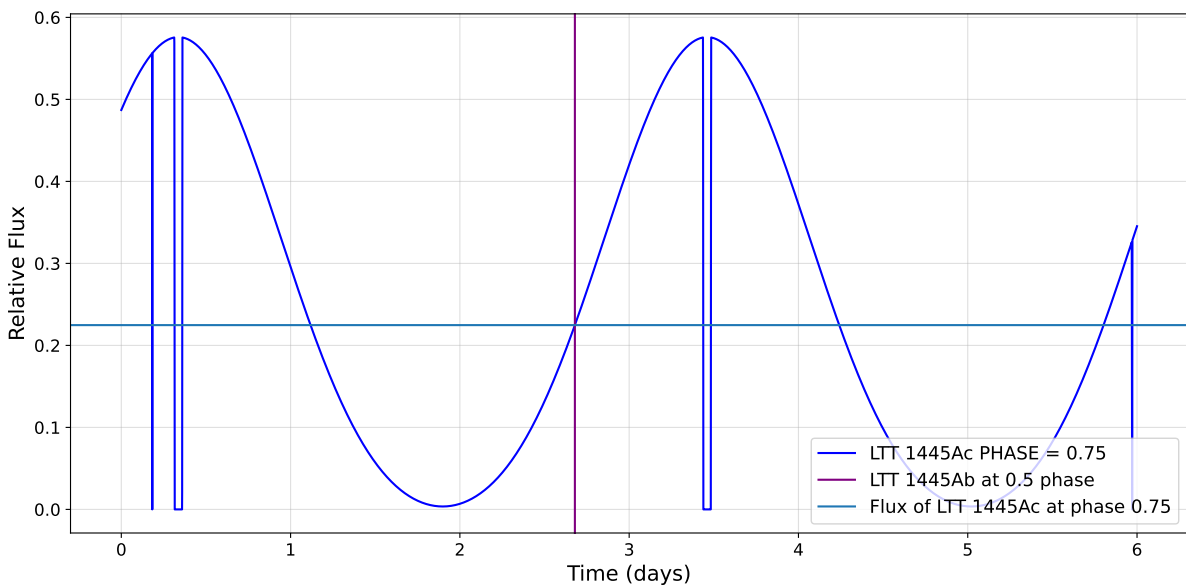

Figure 11: Position test of LTT 1445Ac. This figure is made by setting `t0 = (porb,b * 0.5) + (porb,c * PHASE)` $\simeq 0.6$ phase (for LTT 1445Ac), where `PHASE = 0.75`. This was done to ensure that the PHASE given in the equation sets LTT 1445Ac at the position of that PHASE when LTT 1445Ab is occulting (purple vertical line). To confirm, the light blue horizontal line is the flux value at which LTT 1445Ac is at phase 0.75, showing the intersection of the purple and light blue line, confirming that `t0` is correctly set up.

The test was carried out for multiple phases, and every time the result was the same, the definition of the transit start time correctly sets planet LTT 1445Ac at the given phase at the time of LTT 1445Ab's occultation. In Figure 11, we see the light curve for only LTT 1445Ac; the purple vertical line shows the middle of LTT 1445Ab's occultation. For the transit start time, `t0`, the phase that is set for LTT 1445Ac is 0.75; this means that LTT 1445Ac has just transited and is

at quarter phase, towards occultation. What we can deduce from Figure 11 is that at the point where LTT 1445Ab is occulting, the purple vertical line, LTT 1445Ac is as wanted, at quarter phase, having just transited, and is on its way to occultation. This means that the transit start time is now written in terms of LTT 1445Ab's occultation and LTT 1445Ac's wished phase.

Light Curves

Once the planets, star, and system has been initiated, there are many possibilities to work on the system with `starry`; for example, one could visualize the system by making a video or investigating the light curves. Specifically, the light curves are fascinating, as `starry` can separate the light curves into each object's component that makes up the system light curve. This is particularly interesting, as one can dive deep and investigate each component separately and understand how each object affects the whole and each other. See Figure 12, an example from the start of my project.
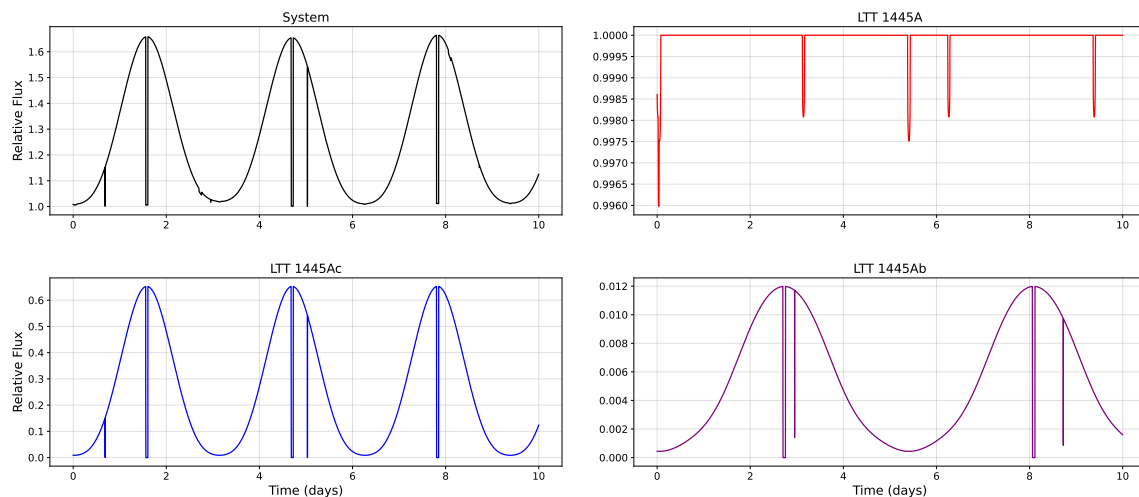

Figure 12: An early example of the different light curves `starry` can produce from my code. The black plot shows the system light curve. The red shows LTT 1445A's light curve; here, we see the transits of the two planets. We also see that the larger planet is LTT 1445 Ab. The blue plot is LTT 1445 Ac's light curve, and the purple plot is LTT 1445 Ab's light curve. On the x-axes, we have the time elapsed in days, and on the y-axes, we have the relative flux.

In order to get these light curves, one needs to define the amount of time the system should run. An example could be that the array spans from time 0 to 10 days; this would mean the system is simulated to span ten days. It is then important to specify how many data points one needs; this indicates to the system how many data points and "where" on the timeline, they should be. It is important to have enough data points; if there are too few, important features of a light curve could go unnoticed, such as an occultation, transit, or even a planet-planet occultation. The time array could look something like `np.array(0,10,10000)`, where we have an array that spans from time 0 to time 10, with 10000 data points. Another exciting feature of the system and light curves is that the system does not need to be run from time 0; one can also

run the system at an earlier or much later time. This way, exploring the system "in the past" or "in the future" is possible.

Wavelength Bins

This project looks at using JWST, and specifically MIRI, which, as mentioned in section 1.5, has different wavelength filters that can be used. For this project, I focused on the following wavelength bins: F1130W, F1280W, F1500W, F1800W, F2100W, and F2550W. I needed to set up the code to include these six wavelength bins. This is possible with `starry`, by including a parameter, `nw`, that defines the number of wavelength bins when setting up the map of the objects. When working with wavelength bins, it needs to be defined for all objects in the system. Thus the star and planets must all have the same number of wavelength bins. This raises a problem in `starry`. It is not possible to include limb darkening on stars while also including multiple wavelength bins with the type of map I used to define the star. I tried to get around this problem but would receive the same error message each time, indicating this was not possible at the time being, to include in `starry`. Therefore I decided to continue making the system with a star that does not consider the limb darkening. This does not skew the results drastically as I focus on secondary eclipses in the infrared, where limb-darkening is negligible, so the analysis remains accurate.

2.2   Model

Creation of Eyeball and Temperature Determination

At the beginning of the project, I worked to get used to the `starry` package and learn how it works. I defined my system manually by finding the values of the parameters from the exoplanet archive and setting in the values when defining the stellar and planetary parameters. Throughout the project, I was introduced to dictionaries and a code snippet that made it possible to directly retrieve system parameters from the NASA Exoplanet Archive (NASA Exoplanet Archive, 2023). This method is much more helpful as the values for the parameters change as new research is done on the system, and these values are updated.

Planets, as we see in our solar system, can come in many different ways. Terrestrial planets in our solar system alone are vastly different from each other. We have Venus, with its very thick atmosphere, and Mercury, without an atmosphere. In my project, I consider the two extreme cases of terrestrial planets. One case is planets that contain very thick atmospheres, so thick that the atmosphere completely redistributes the radiation from the star. The other case is the airless, no atmosphere planets, where all the radiation is re-radiated immediately. Keep

in mind that the planets I am looking at are most likely tidally locked, meaning the same side of the planet is facing the star. For the thick atmosphere case, the tidally locked planet is not affected as much due to the total redistribution of the radiation. The tidally locked planet is significant for the no atmosphere case, as this means that the no atmosphere planet will have a permanent hot spot at the sub-stellar point (the point where the stellar radiation is "straight overhead"). For the remainder of the thesis, I will refer to the thick atmosphere case, where the radiation is redistributed, as the atmosphere case. I will also refer to the airless permanent dayside case as the no atmosphere case. The atmosphere case is straightforward, as the ydeg for the planets is set to 0, meaning the surface map of the planet is uniform. The no atmosphere case proved to be more challenging, as I needed to create the characteristic eyeball surface map, as can be seen in Figure 2. I first attempted to play with the spherical harmonics, setting ydeg = 5 and defining the "amount" each spherical harmonic degree contributes to the overall map manually. Initially, I would get a "too small eyeball," meaning part of the night side (the side that faces away from the star) bled onto the dayside. See Figures 13a and 13b.

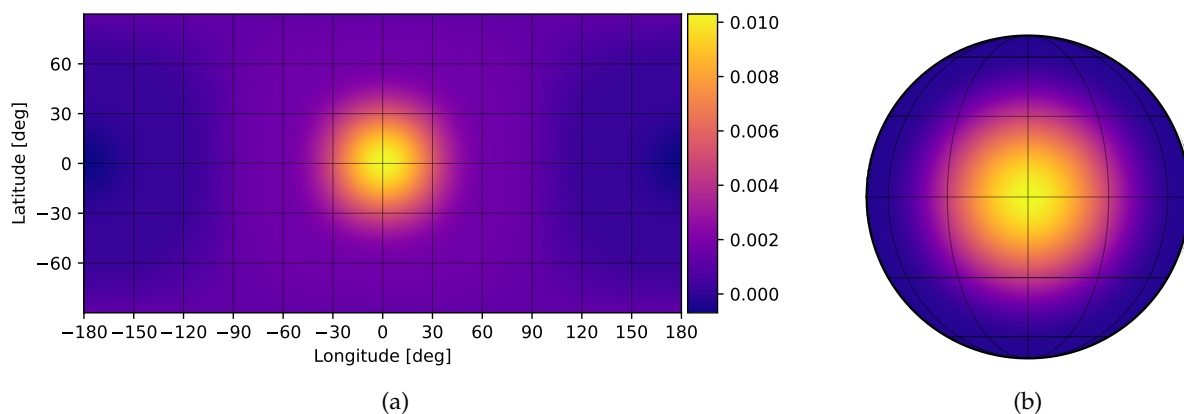(a)   (b)

Figure 13: The surface map of the eyeball planet I created using spherical harmonics. It is important to notice that the eyeball does not reach as far as needed.

Further into the project, I discovered that with starry, it is possible to use a function called spot. This was in the context of creating a star with a sunspot, but I used the same function and inverted the amplitude so that instead of creating a "cold spot," I created a "hot spot." This spot method proved to be much easier, as I could specify where the spot should be located and how large it should be. Through trial and error, I created a spot much more realistic to the "eyeball" case than what I created with the spherical harmonics; see Figure 14a and 14b.

The result was that I successfully created two cases for the planets: a thick atmosphere case, where the radiation is totally redistributed around the planet, and another where the planet is void of an atmosphere, with the recognizable eyeball surface map. I used the equilibrium temperatures from Winters et al. (2022) for the equilibrium case. This temperature was used over the whole planet's surface, meaning the dayside and night-side of the planet have
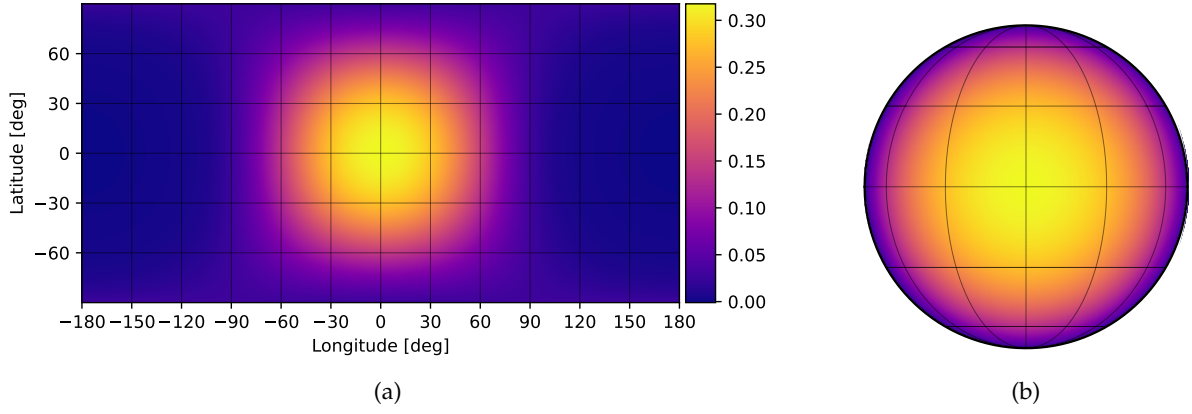
Figure 14: This figure shows the surface map of the eyeball planets, created using the spot method. Compared to Figure 13, this method gives a much better result, where there is much less "night-side" bleeding onto the dayside.

the same temperature. This is due to the total redistribution of radiation in the planet's supposed atmosphere. The permanent sub-stellar temperature, or the temperature for the planets with no atmosphere, has yet to be observed and calculated. Therefore I take a more theoretical approach and calculate the supposed dayside temperature of the planets. To calculate the dayside temperature, we use the following equation:

$$T_{day} = T_\star \sqrt{\frac{R_\star}{d}} (1 - \alpha_B)^{1/4} f^{1/4} \tag{2}$$

The equation uses the stellar temperature and radius, the planet's semi-major axis, d, the Bond albedo, α_B, and f is the heat-redistribution factor. The Bond albedo is assumed to be that of the most extreme case; therefore I set it to 0, as this indicates that all the radiation is absorbed. The heat-distribution factor has two limits; $f = 2/3$ for instant re-radiation, which is relevant for the eyeball case, or $f = 1/4$ for a uniform redistribution, and this is the case for the equilibrium case, as all the radiation is transported uniformly around the planet (Koll et al., 2019). To test the equation, I calculated the equilibrium temperature with the above equation using $f = 1/4$, resulting in the same temperature as in the paper. I provide the equilibrium (atmosphere) temperature case and the permanent dayside or eyeball (no atmosphere) case in the following table:

Planet	T_{eq}	T_{day}
LTT 1445Ab	424 K	542 K
LTT 1445Ac	508 K	649 K

Later on, I created a function that would take the planet's temperature as one of the variables, determining if the function gave the planet the spot or if the planet would have a uniform map. It would do this by taking the temperature passed in the function and comparing it to the

dayside temperature of the planet; if the temperature was larger than the limit, the spot would be added; if the temperature was lower, no spot was added.

```
if T > Tday,p - 10:

    planet.map.spot(contrast = -1, radius = 60)
```

Here, T is the passed temperature (either the equilibrium or the dayside temperature), and Tday,p is the dayside temperature.

The star has a uniform surface map, just like the planets in the equilibrium case. This means the ydeg = 0. I chose this as I am not interested in seeing how possible starspots and other features of the stellar map can affect the result. Initially, I also included the limb-darkening parameter udeg and found the corresponding value for LTT 1445A, but as mentioned, I removed this when I introduced the multiple wavelength bins. Next, I create the system and run it over time to test if it is working. When starting, I created a system with just one planet to ensure I defined the planets and system correctly. I added the second planet once I determined the system, and the light curves with just one planet looked satisfactory. The system was set up correctly with two planets, and my understanding of this basic code was sufficient to start playing around with the multiple wavelength bins. I created random wavelength bins to test and understand how this works. With the multiple wavelength bins, I could change the amplitude of the object for each bin. I moved forward to understand how the wavelength bins and the amplitudes could be utilized.

Amplitude Correction

Upon investigating and looking at examples, I found that I can manually set the amplitude and define the amplitudes for each wavelength bin individually. When initiating the planets, one sets up the planets with an initial amplitude; this can be updated later. With some tests of simple amplitudes, I found that by defining an amplitude array that mirrors the number of wavelength bins, I can set the amplitudes for each wavelength bin. With the test done and understood, I worked on figuring out the correct amplitudes I should use. Initially, I used the blackbody radiation function and created the blackbody for the planets, and for each wavelength in the bins, I would take the value the corresponding planet had on the blackbody plot.

Later on, I found that another way that could work is to look at the $\frac{F_{planet}}{F_{star}}$ plots. These plots look at the planet's flux normalized to the star's flux over different wavelengths. Figure 15, shows my $\frac{F_{planet}}{F_{star}}$ plots, for several different situations. LTT 1445Ab is represented with purple colored lines, and LTT 1445Ac is represented with blue colored lines. The solid lines are the
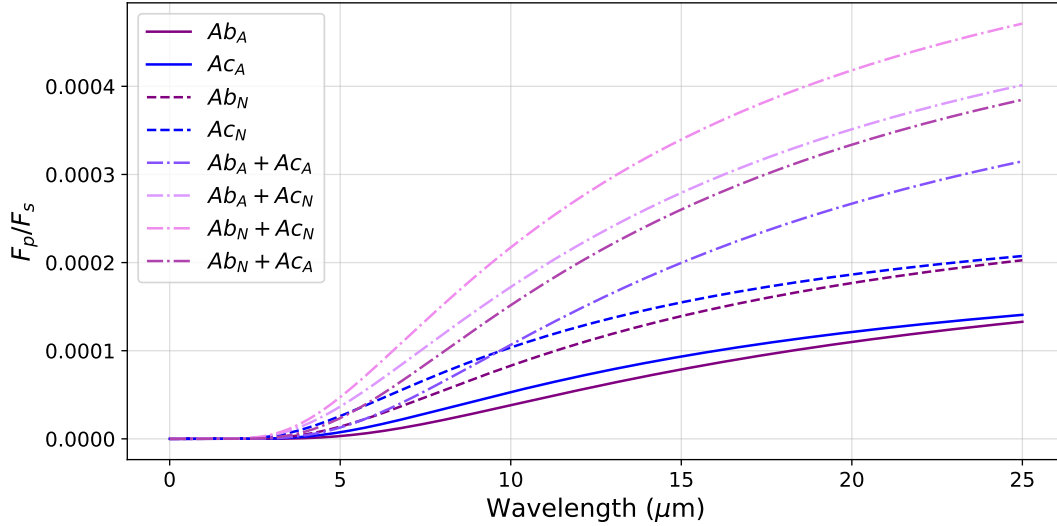
Figure 15: Planetary Flux over Stellar Flux as a function of wavelength (μm). Planet LTT 1445Ab are the purple lines, and LTT 1445Ac are the blue lines. The solid lines are the atmosphere case, and the dashed lines are the no atmosphere case. The dashed-dotted lines combine both planets in secondary eclipse, with either an atmosphere or not. Noticeably, the larger the wavelength, the more of a separation between the different cases. This is important for my thesis, as it is this difference I want to find in the simulated data.

atmosphere cases for either planet, whereas the dashed lines are the no atmosphere cases for either planet. The dashed-dotted lines are the combination of both planets, where each color is a different combination of either type of planet. Noticeably, the larger the wavelength, the more of a separation between the different cases. This is important for my thesis, as it is this difference I want to find in the simulated data. Initially, I set the amplitudes for each wavelength bin to the given value from the F_P/F_S plot for the individual cases.

I worked with this for a while but then discovered through my phase plots of the planets that the amplitudes were not doing what I intended. The intention with this was that for the no atmosphere case, the amplitude, as seen in figure 15, would be the amplitude of the hot spot on the planet, the substellar point, and the amplitude for the no atmosphere case, would be the amplitude all over the planets. It seemed that `starry` has a specific way of working with the amplitudes, and in order to make the amplitudes what I intended, I did some tests and found a solution. I found that if I normalized the amplitude to the predicted flux values I calculated, the result would be the amplitude of the hotspot for the no atmosphere, and the uniform atmosphere case would be identical to that I calculated. See Figures 16, 17, for the phase map plots for LTT 1445Ab. When comparing the figures to table 1, one can see that the values match, and thus I have correctly set the amplitudes to what I have intended.
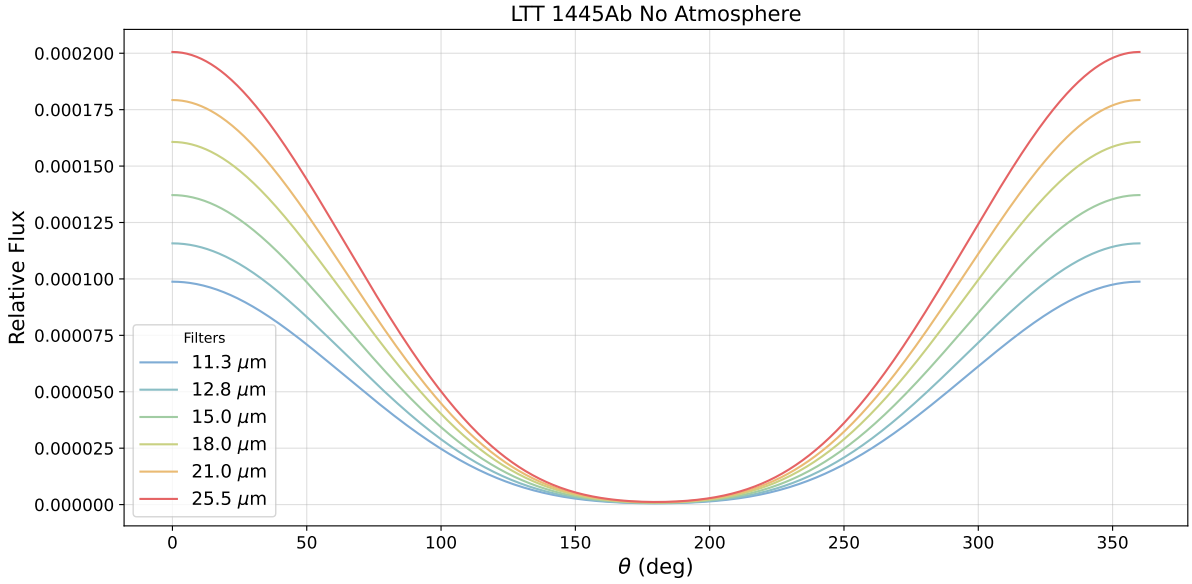
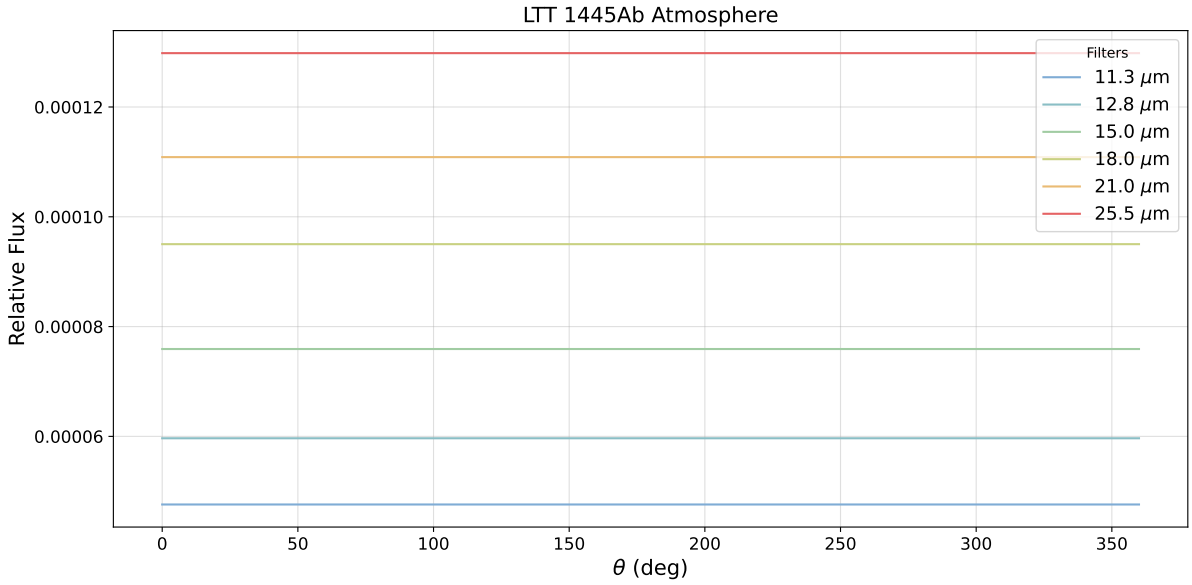Figure 16: The phase map of the planets' surface in the different filters, for the no atmosphere case.

Figure 17: The phase map of the planets' surface in the different filters, for the atmosphere case.

Planet Flux	11.3 μm	12.8 μm	15 μm	18.0 μm	21.0 μm	25.5 μm
No atmosphere	9.877e-05	1.157e-04	1.371e-04	1.606e-04	1.792e-04	2.005e-04
Atmosphere	4.759e-05	5.965e-05	7.591e-05	9.501e-05	1.108e-04	1.298e-04

Table 1: Values of the maximum flux for LTT 1445Ab for both the atmosphere and no atmosphere case for the different wavelengths as calculated from the blackbody curve for LTT 1445Ab. The values in this table match the maxima of Figures 17 and 16.

Model Light Curves

Figure 18, shows the final model light curves. These light curves are made after the system is set up, and the correct measures are taken to ensure the amplitudes for each wavelength bin are set. The figure shows the light curve for the whole system, meaning this is the model light curve one would receive if there is no error in the observations. The figure shows LTT 1445Ab occulting, and LTT 1445Ac is at phase 0.3 at the midpoint of LTT 1445Ab's occultation.
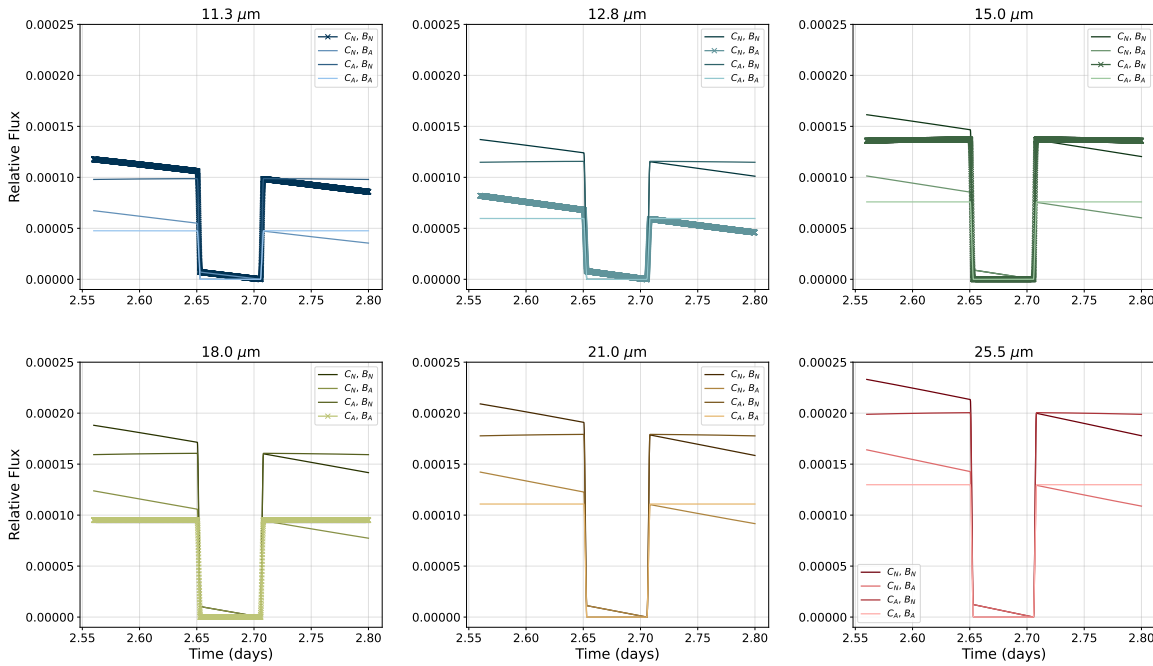

Figure 18: A figure showing light curves for six different wavelength bins with four different planet configurations. The color code follows that of the MIRI instrument filters as seen in Figure 7. Furthermore, for each subplot, the gradient goes as follows: The darkest color shows the most extreme case, that of both planets with no atmosphere. The next darkest shows the curve for when LTT 1445Ac has no atmosphere, and LTT 1445Ab has an atmosphere. The second lightest color is for the case where LTT 1445Ac has an atmosphere, and Ab does not. The lightest color shows the case of both planets with an atmosphere. Notice that when at least one planet has an atmosphere, there is a significant increase in flux. Furthermore, the shape of the occultation also shows some variability concerning if Ac has an atmosphere or not.

Figure 18 presents model light curves for the different wavelength bins, and within each wavelength bin, there are four light curves, depending on the planetary setup. The colors mirror the filter colors that have been used throughout the thesis. The darkest shade in each plot represents the no atmosphere for both planets' case. The next darkest shows the light curve for LTT 1445Ac has an atmosphere, but LTT 1445Ab does not. The second lightest color indicates the situation where LTT 1445Ac has no atmosphere, but LTT 1445Ab has an atmosphere. Lastly, the lightest color represents the light curve for the situation where both planets have an atmosphere.

It is interesting to notice the shape of the occultation when LTT 1445Ac has no atmo-

sphere; we see a slope at the bottom of the occultation. Comparing this to the situations where LTT 1445Ac does have an atmosphere, we do not see this slope. Furthermore, the depth of the occultation depends on whether LTT 1445Ab has an atmosphere or not, yet the shape of the occultation depends on LTT 1445Ac containing an atmosphere. Another important factor is the extreme case, seen as the darkest colored plots; it shows that the overall flux is significantly larger than the case with both planets with atmospheres (the lightest colored plots). This is a particularly exciting outcome that the models show this significant change depending on the properties of the planets. The next question is, is this difference in the cases an observable effect when considering the error and scatter of the data?

2.3 Simulated Data

JWST & Pandeia

The simulated data starts with the models previously made with `starry`. The models must then be altered to mirror what one would observe with JWST. When I started the process of making simulated data, I worked with adding an arbitrary scatter to the model. This was to understand how I could create a normally distributed scatter. Once I understood how to add scatter to the data, I calculated the correct scatter. I used Pandeia, a powerful exposure time calculator tool, to do this. I was given a code snippet that calculates the necessary information within my code, rather than using the GUI from https://jwst.etc.stsci.edu/. The code starts with retrieving the sky background from the JWST backgrounds database; this is dependent on the system coordinates. Next, MIRI dictionaries are created, including a calibration dictionary. The last bit of the code makes the necessary calculations; from the Pandeia code, we want to get the integration time, t_{int}, the cadence, and the standard deviation, σ. The integration time is the time that the instrument gathers the photons; in other words, how long it takes it to take one little observation. The cadence includes the "extra" time needed to read out the observation. Lastly, the sigma, or the standard deviation, is the noise/flux. This will be used to get the correct scatter around a normalized flux level. The integration time and the cadence will be used to calculate the possible points in the given time to be observed so that the integration time and readout time are considered. This ensures that the simulated data represents the real situation as best possible.

Scatter

With the standard deviation calculated, the scatter can be implemented on the model to create the simulated data. The scatter is made to follow the normal distribution, thus when I initially made the first test to add the scatter, I set up the scatter as seen in Figure 19.

```
''' Make the simulated data, as would be seen from JWST '''
flux_d_a_a = []
flux_d_a_n = []
flux_d_n_n = []
flux_d_n_a = []

for i in range(0,len(target['calc']['filters'])):
    flux_d_a_a.append(flux_t_a_a[i] + sigmas[i] * np.random.randn(len(t[i])))
    flux_d_a_n.append(flux_t_a_n[i] + sigmas[i] * np.random.randn(len(t[i])))
    flux_d_n_n.append(flux_t_n_n[i] + sigmas[i] * np.random.randn(len(t[i])))
    flux_d_n_a.append(flux_t_n_a[i] + sigmas[i] * np.random.randn(len(t[i])))
```

Figure 19: A snippet of my code showing how the simulated data is set up.

`flux_t_a_a` stands for the flux of the model (theoretical/model = t) for the system with both planets containing atmospheres (atmosphere = a, no atmosphere = n). I take the corresponding standard deviation for the filter and multiply it by a random number that follows the normal distribution. The flux for the simulated data is thus created by taking the theoretical or model flux and adding a random scatter.

At first, I created a random seed to ensure all the scatters were identical. With this method, I received some perplexing results, leading me to do more tests with the scatter and the random variable. My tests include a situation where for all the different phases of the planets in their orbit, the scatter would be the same, but for each of the different wavelength bins, this scatter would change. The other test situation was that the scatter would be entirely different for all phases and all wavelengths. The latter situation leads to more realistic results; due to the nature of actual observations, the scatter would be different for each observation, and one would not get two observations that were the same. Thus intuitively, it makes sense to choose this situation to define the scatter of the simulated data. With that being said, part of my test is to see which phase of LTT 1445Ac will match the models the best, and for this case, keeping the scatter the same for the different phases but altering it for the different wavelength bins makes the most sense for the analysis. To get the whole picture, I made the simulated data and the analysis for both scatter situations.

Binning

Another important factor to keep in mind is the binning. Binning pertains to taking data points in time bins and then making a new binned data point. This can aid in making the data much less "noisy" and make the data clearer. Figure 20 shows the simulated data before binning. As can be seen, the figure is not very enlightening, as there is too much scatter in the data. One must be meticulous when binning, as over-binning can lead to losing important information. This I found out when testing the binning factor, and would end up with no occultations or transits due to the excessive binning. To combat this, I bin the data by first

calculating the transit time. This is the time it takes the planet to transit from t_{II} to t_{III}, see Figure 21.
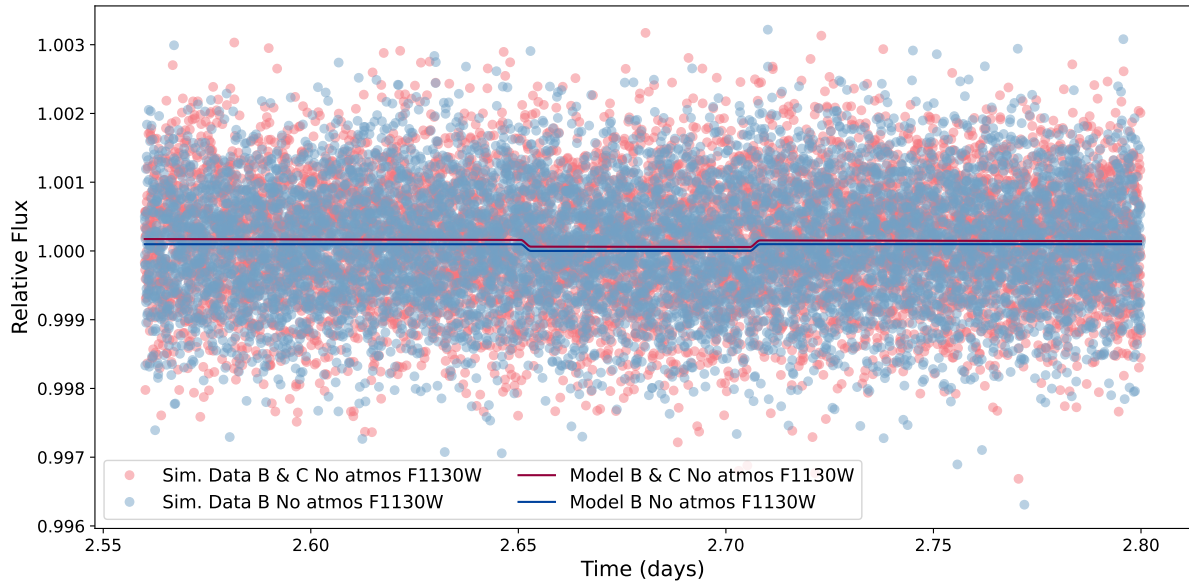

Figure 20: This figure shows the light curve of the system, as "raw" simulated data. Thus meaning the simulated data is unbinned. We have the relative flux on the y-axis and the time in days on the x-axis. Without binning the simulated data, it is very hard to see any patterns and get any information from this figure.
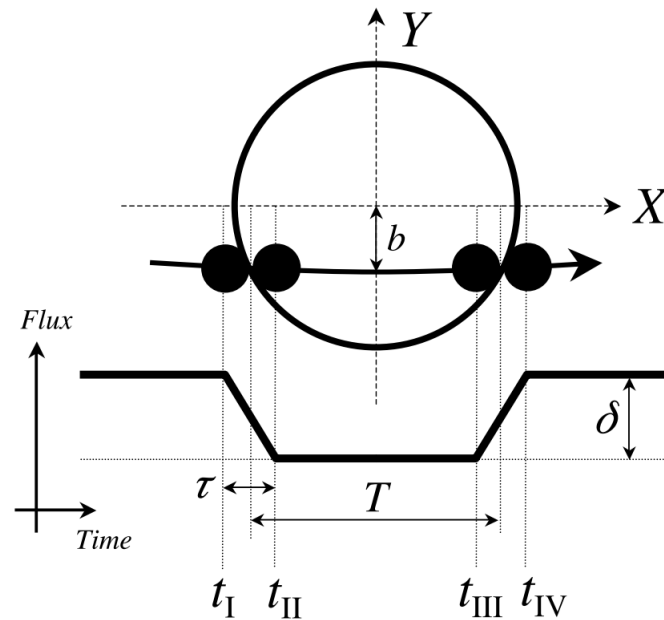

Figure 21: This image shows an illustration of a transit, indicating where the different contact points are. When I bin the data, I take the time between t_{II} to t_{III}, and divide by 5, to make sure that in this part of the transit, there are 5 data points. Figure from Winn (2010)

With the transit time calculated, I divided this time into 5, as I want to have at least 5 data points in the middle of the transits/occultations to ensure sufficient sampling. Figure 22 shows the binned data.

30
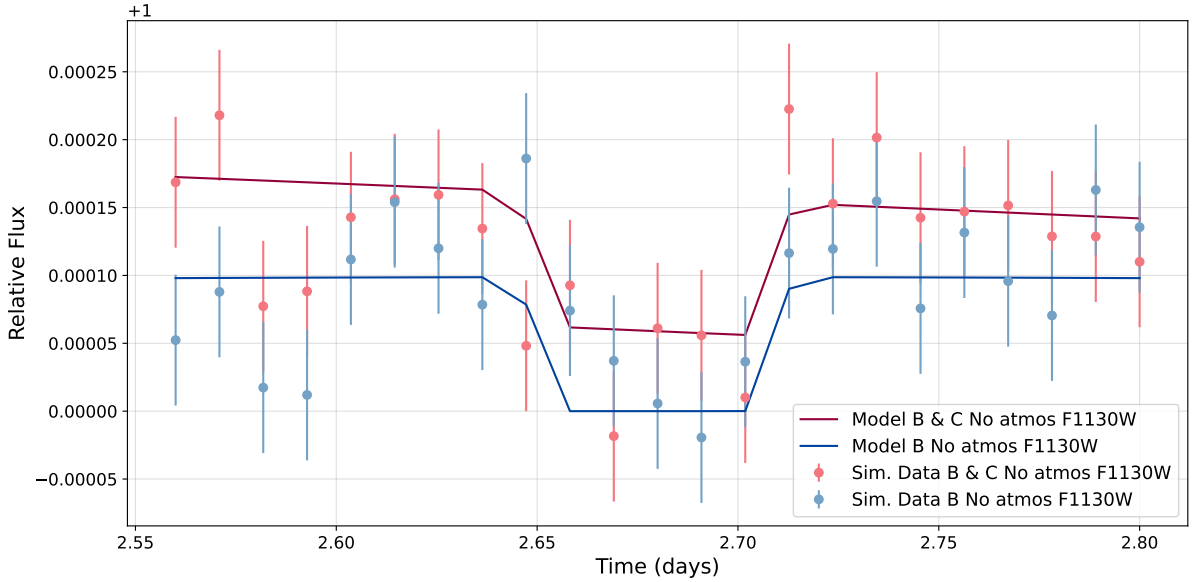
Figure 22: This figure shows figure 20, after it has been binned. Here we notice that the blue data points and model are displaced lower than the red. This is the unscaled binned light curve.

Error Propagation

After binning, it is important to still portray the information that has been converted when binning. This can be expressed as error bars on the data points. I perform error propagation, where I calculate the error with the following equation:

$$Error_{binned} = \frac{\sqrt{\sum_N \sigma_i^2}}{N} \tag{3}$$

The error is calculated by taking the sum of the squared standard deviations of each point, and taking the square root of this, then dividing by the number of points. Due to the standard deviations not changing in my simulated data, I can simplify equation 3 to the following:

$$Error_{binned} = \frac{\sqrt{\sigma^2 N}}{N} \tag{4}$$

With the error calculated, I can add it to my data points; this is what we see in Figure22.

2.4   Statistics

Scaling

When working on the model and further on the simulated data, I noticed that the flux was significantly lower for planets with an atmosphere. Thus when performing a statistical analysis on the simulated data versus the models, the result would not be enlightening, as it is obvious

31

to notice that the model that includes two planets with no atmospheres as compared to a model with one planet with or without an atmosphere, would fit much better to the simulated data that portrays the situation with two planets with no atmospheres. Therefore it was essential to scale the one-planet models and simulated data so that they are at the same scale as the two-planet models and data in order to give the most reliable data analysis. I found the differences between the models with one planet and those with two planets to calculate an offset to scale the models and the simulated data for the one-planet case.
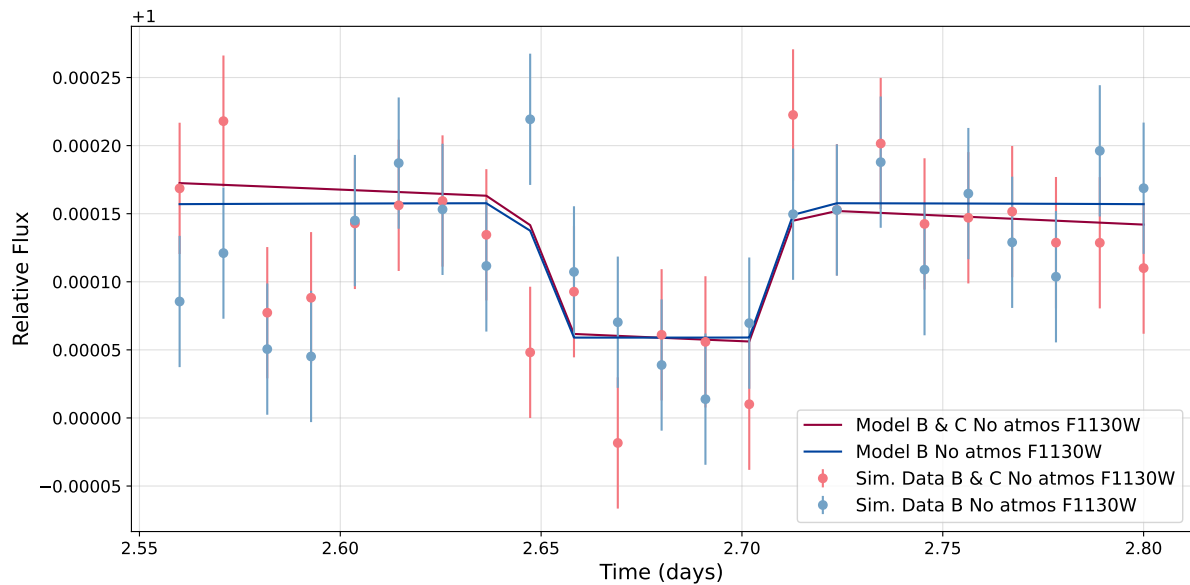
Figure 23: This figure shows figure 22, after I have scaled the single planet model, there is no significant difference in the relative flux.

Figure 23 shows the effect of scaling the data on the plots. Once the scaling has been correctly implemented, further analysis of the different simulated data cases and the models can be carried out.

Comparison of F1130W and F2550W

To illustrate the difference between two wavelength filters, Figure 24 shows two light curves of wavelength bins F1130W and F2550W with the respective errors. The plots have the same y-axis, thus showing that the 25.5 μm filter has a significantly larger signal but with accompanying large error bars. Note the light curve for the F1130W filter differs from the similar light curve in Figure 23, but due to rerunning the code, the randomness of the scatter is slightly different.
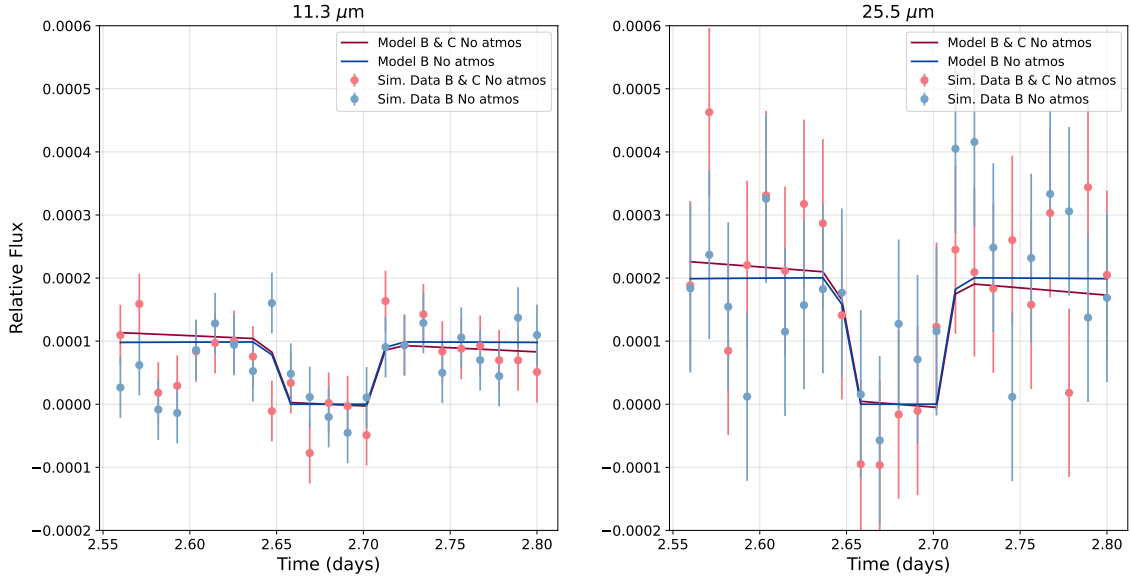
Figure 24: A comparison of two filters, F1130W and F2550W. This figure illustrates the significant increase in the error of F2550W, despite the filter also having a larger signal, the noise is also larger when comparing to other filters.

Chi Square Test

The first method of statistical analysis I explored was a chi-square test. This analysis method compares the data to theory using a simple mathematical expression. The following expression calculates the chi-squared, χ^2,

$$\chi^2 = \sum_i \left[\frac{y_{ob_i} - y_{th,i}}{\sigma_i} \right]^2 \tag{5}$$

The chi-square test takes the deviation of the observed data point and the theoretical data point, divides this by the standard deviation, and takes the square of the result. This is then done for all data points and summed. Once the chi-square is calculated, one can take the chi-square test. This takes the calculated chi-square and the degrees of freedom and can indicate if the model's fit is sufficient or too good/bad. The degrees of freedom is the difference between the number of data points, n, and the number of free parameters, p, $f = n - p$. The answer to the chi-square test is more so an answer of probabilities rather than a yes or no answer (Bradt, 2003).

Bayesisan Information Criterion

The Chi-square test method did not favor the type of statistical analysis I wanted to complete for this research. I wanted a way to compare the statistical likelihood of the two models. For this purpose, the Bayesian Information Criterion (BIC) is a better statistical analysis method. Using Bayes' theorem, this statistical analysis tool computes the probability that one

of the theories (models) is preferred over another. The BIC is defined as:

$$BIC = k \cdot log(n) - 2 \cdot log(L(\theta'))$$
(6)

Here k is the number of parameters, also known as the degrees of freedom. The degrees of freedom are the free parameters that can change or not be constricted by the model. In my case, I counted these and set the number of parameters accordingly. Next, n is the number of points in the data. This is calculated for each of the wavelength bins. Lastly, there is L, the likelihood function. This is a type of joint probability of the observed data as a function of a statistical model. For my statistical analysis, this model is a Gaussian model. I set up the likelihood function as follows:

$$-\frac{n}{2}log(2\pi) - \frac{n}{2}log(\sigma^2) - \frac{1}{2 \cdot \sigma^2}\sum(data - model)^2$$
(7)

Here n is the number of points; sigma (σ) is the noise or the error applied to the data. Lastly, we have the sum of the difference between the data and the model (Schwarz, 1978).

Then I calculated the BIC values for various situations, such as the data of the two-planet system against the model of the two-planet system and another situation of data of the two-planet system against the model of the one-planet system (just LTT 1445Ab). This was done for all the configurations possible to implement in the system, meaning the BIC values have been calculated for the most extreme system of both planets containing no atmospheres and until the least extreme case of both planets containing atmospheres. Once the BIC values have been calculated for the different situations, I then take the difference of the BICs, for example, the BIC value of the data of the two-planet situation against the one-planet model subtracted by the two-planet data against the two-planet model. I then get the difference between these two BIC values, and depending on the value, it can show if the result is significant or not.

According to Lorah & Womack (2019), if the difference is greater than 10, this indicates very strong evidence, a difference between 6-10 indicates strong evidence, between 2-6 indicates positive evidence, and lastly, a difference between 0-2 indicates weak evidence. In the case of the above example of comparing the two-planet data against the one-planet model, subtracted by the two-planet data against the two-planet model, if this gets a BIC difference value greater than 10, this indicates that the data fits the two-planet model better than the one planet model. In other words, the lower the BIC value, the better. For the hypothesis to be confirmed, I am looking for my results to show high BIC difference values, ideally a difference of greater than 10.

3 Results

To remind you of the purpose of this thesis, I perform two tests to explore the hypothesis that the sibling planet LTT 1445Ac can affect the observed signal of LTT 1445Ab. I have set up a code that accurately simulates the received signal of the system, which produces light curves for the six MIRI filters. I performed two tests by changing two different aspects of the system to see what effect would have on the signal. The first test I perform is to change the position of LTT 1445Ac in its orbital phase and examine to what extent, if any, the position of LTT 1445Ac makes it possible to distinguish in the signal that there are two planets and not just one. In other words, if there is a point in LTT 1445Ac's phase where the two-planet model fits much better than the one-planet model. If there is a favorable phase, this will be used to continue with the next test. The next test examines whether changing LTT 1445Ac's position, or semi-major axis, can induce a noticeable change in the signal.

Changing Phase of LTT 1445Ac

I set up the code to change the orbital phase of LTT 1445Ac. I decided to change the phase in increments of 0.05. It is important to note that the results are slightly skewed at orbital phases corresponding to transit and occultation of LTT 1445Ac (0.5 and 1 or 0), as the signal given would not be possible with just a one-planet model. Specifically at transit, the two-planet model is necessary, as it is known that LTT 1445Ab is at occultation, and thus the absence of flux can only be due to a second transiting planet, LTT 1445Ac.

As mentioned before, the scatter was highly debated whether keeping the same scatter in the phase changes but differing with each filter, or having a completely random scatter for all phases and filters, would be the right way forward. I decided to run my results for both cases. I will first show the completely different scatter for all phases and wavelengths. Figure 25 shows the difference in BIC as a function of the phase of LTT 1445Ac. Plot a) shows the whole plot, and plot b) shows a zoomed-in version of plot a).

In the next case, the scatter is the same for each phase and different for each wavelength. Figure 26 shows the same plots as 25, with a different scatter situation. When keeping the same scatter for each phase change, the result is more enlightening, showing the effect of changing the phase and how well the models fit the data. From Figure 26, it can be seen that at phase 0.3, there are three filters (F2100W, F1280W, and F1500W) that show positive evidence of the two-planet model fitting the data better. Therefore I decided, for the next test, to keep the phase at 0.3 when changing the semi-major axis.
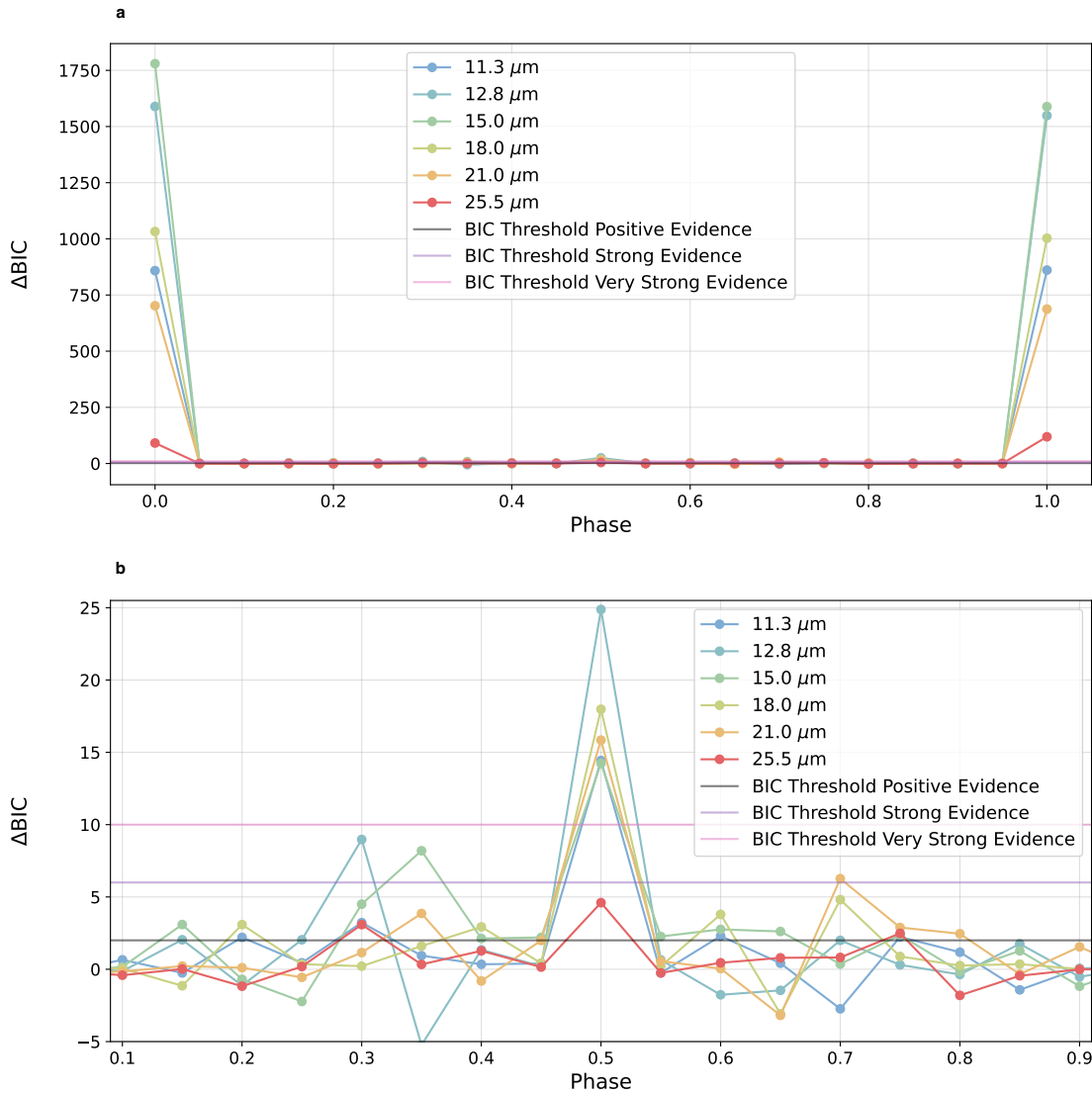
Figure 25: This figure shows the BIC difference of the two-planet model vs. the single-planet model (only LTT 1445Ab) as a function of the orbital phase for each wavelength filter. This is for the scatter situation, where the scatter differs for each phase and filter. Plot a) shows the full figure, and plot b) shows the zoomed-in plot. The results indicate some significance, specifically for phases 0.3 and 0.7.
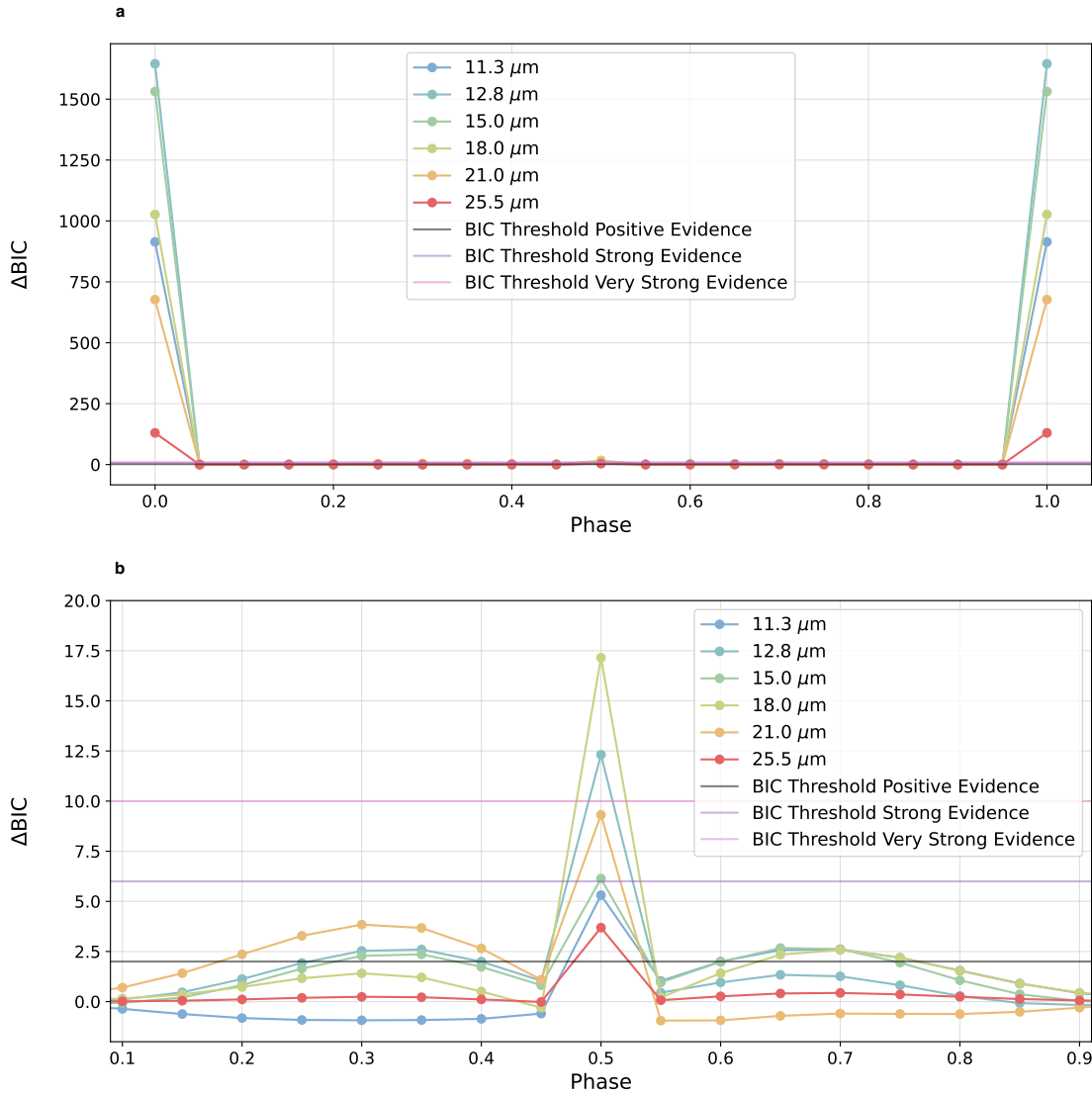
Figure 26: This figure shows the BIC difference of the Two planet model vs the single-planet model (only LTT 1445Ab) as a function of the orbital phase for each wavelength filter. This is for the scatter situation, where the scatter is the same for each phase and different for each filter. Plot a) shows the full figure, and plot b) shows the zoomed-in plot. The results indicate the most significance in the phase of 0.3 when overlooking the occultation and transit phases (0.5 and 1 & 0)

Changing semi-major axis, *d* of LTT 1445Ac

The result from the first test showed lots of weak evidence for the two-planet model fitting best. There was positive evidence for a few wavelengths, mostly at orbital phases 0.3 and 0.7. Similarly to the previous test, I will change the scatter from entirely different to the same over the changing distances. First, I will show the result of the scatter being completely different over all distances and filters.

The range of orbital distances I have chosen goes from the actual orbital distance of LTT 1445Ac at 0.026 AU down to the shortest orbital distance I could find. I found that the second shortest orbital period known thus far is K2-137b, a transiting terrestrial exoplanet orbiting an M-dwarf. K2-137b orbits its host star in just 4.3 hours, losing the first spot of the shortest orbital period known by 4 minutes to KOI-1843.03 (Smith et al., 2018). The orbital distance of LTT 1445Ac at 0.026 AU gives an orbital period of 72 hours. Furthermore, an orbital period of 4.3 hours gives an orbital distance of 0.004 AU. Therefore, I have set the range from 0.004 AU to 0.026 AU, with orbital periods from 4 to 72 hours.

It is clear to see from the first plot in Figure 27 that the closer the secondary planet is to the host star, the two-planet model is a much better fit. It is hard to see the result at more considerable distances in plot a); therefore, in plot b) in Figure 27, we see the zoomed-in plot. Next, I show the results with the scatter unchanging for each distance. See Figure 28 for the full figure and the zoomed-in plot. For the different scatter analysis, at larger orbital distances, certain filters show better results, although almost all filters have some degree of significance. At an orbital distance of 0.016, all filters show very strong evidence of a two-planet model fitting the simulated data best. For the same scatter situation, we see lesser significance at larger orbital periods, and a lower orbital distance is needed for all of the filters to show strong evidence when compared to the different scatter cases.

I also completed the analysis for the system configuration where LTT 1445Ab has an atmosphere and LTT 1445Ac does not. These results can be seen in Appendix 3, in Figures 48 and onward. The results of these are very similar to those of the case shown. I decided to completely omit analyzing the situation where both planets have an atmosphere due to there not being a difference in the light curves, as I have scaled the results and thus would show results of no significance. I refer to the light curve in Appendix 1, Figure 33, where there is no difference between the two models and the data.
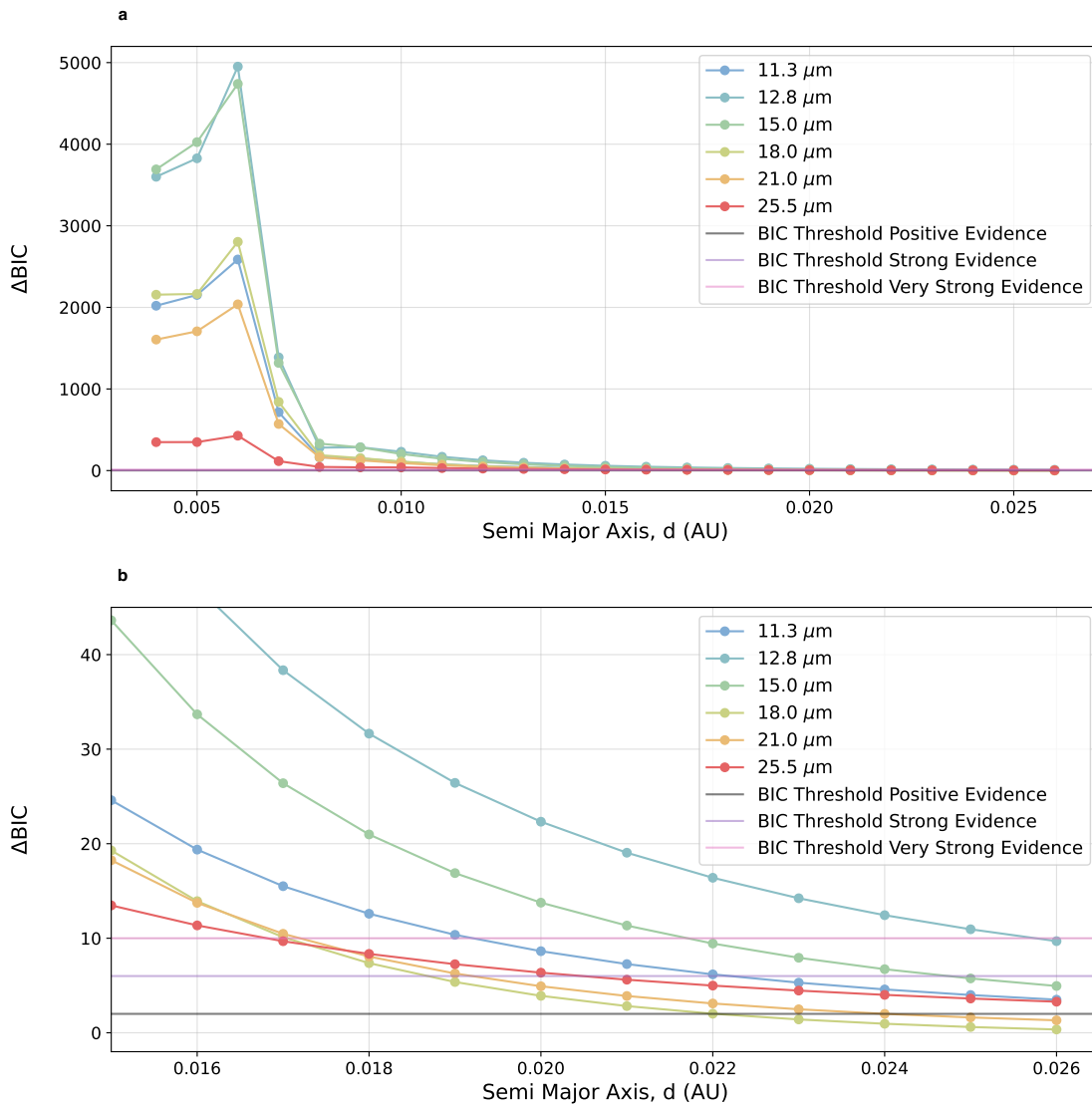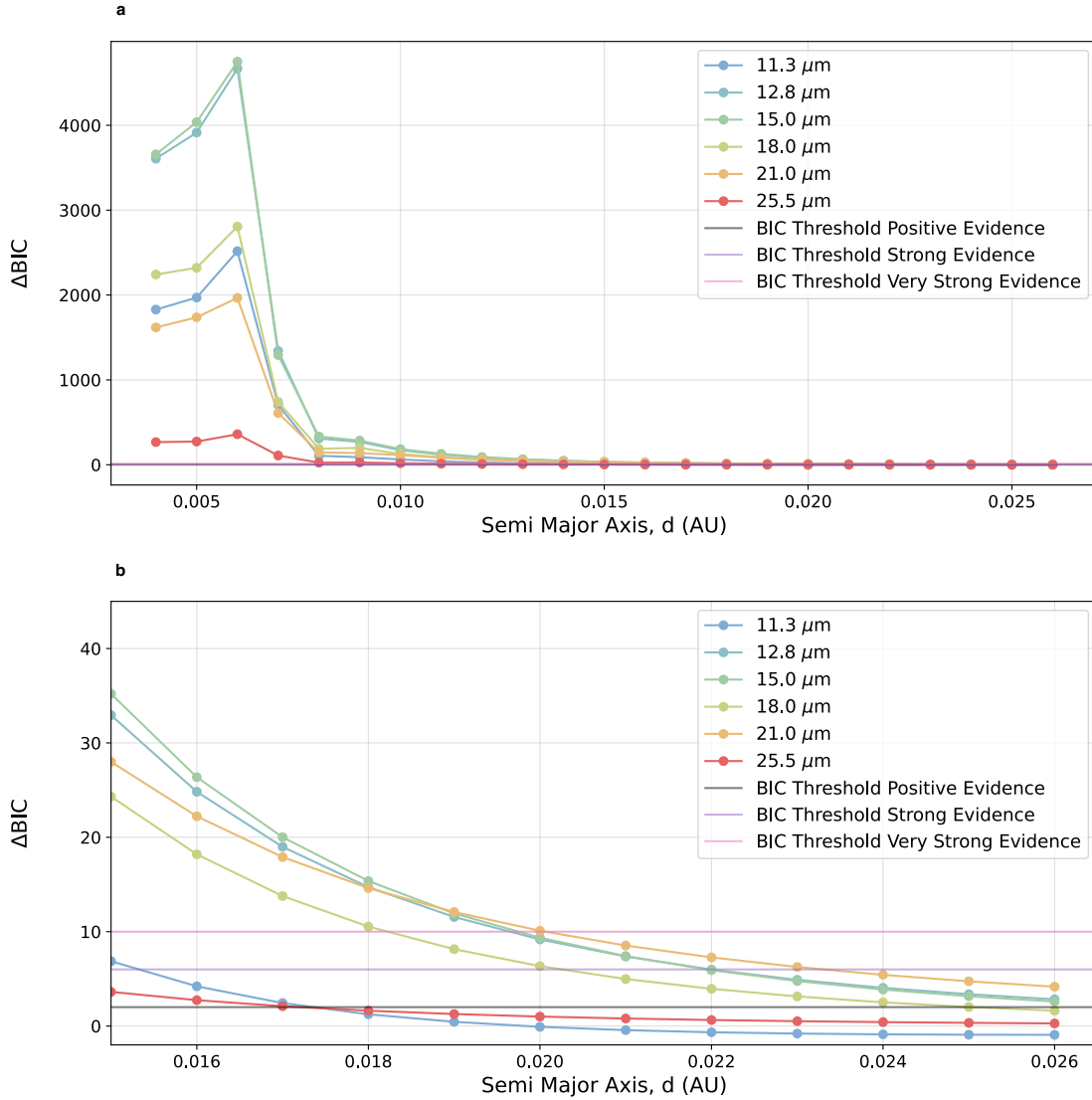
Figure 27: This figure shows the BIC difference of the two-planet model vs. the single-planet model as a function of the semi-major axis for each wavelength filter. This is for the scatter situation, where the scatter differs for each phase and each filter. a) Zoomed-out plot, b) Zoomed-in plot. We see positive to very strong significance ($\Delta BIC > 2$) already at the correct semi-major axis of 0.026 AU. The significance only increases as LTT 1445Ac moves closer to the host star.

Figure 28: This figure shows the BIC difference of the Two planet model vs the single-planet model as a function of the semi-major axis, for each wavelength filter. This is for the scatter situation, where the scatter is the same for each phase and different for each filter. a) Zoomed-out plot, b) Zoomed-in plot. We see positive significance (ΔBIC >2) already at the correct semi-major axis of 0.026 AU for the filters F1280W, F1500W, and F2100W. The significance only increases for all filters (except F1130W and F2550W) as LTT 1445Ac moves closer to the host star. Only much closer to the host star do filters F1130W and F2550W start showing significance.

4 Discussion

Through setting up the exoplanet system LTT 1445A, producing several configurations of the system, and testing each configuration, the question of: *Is it possible to distinguish if a planetary sibling can have a significant effect on the signal, to be able to detect it, and distinguish if there is an atmosphere or not*; has been thoroughly investigated. The tests I performed considered the kind of scatter one would get when observing the same system multiple times (completely different scatter) and another that is less realistic but better for the analysis (same scatter). The results show that when observing the exoplanet system LTT 1445A, certain phases of LTT 1445Ac indicate one can distinguish from the signal that there is certainly a secondary planet, specifically a secondary planet that contains no atmosphere. Interestingly, we see more positive and strong evidence to support the two-planet model when the scatter is entirely different, as in Figure 25. With that taken into account, and the result of Figure 26, the conclusion I take is that the phases 0.3 and 0.7 are the phases at which one would have the best chance of being able to distinguish with some degree of certainty that the observed signal could have traces of another planet. This makes sense as the planet is facing the dayside towards the observer. When looking at the filters, we see a less prominent trend; for example, in figure 26, the filter that shows the best evidence is the orange, 21 μm filter. However, when comparing to 25, this is not the case; it is one of the least significant filters for phase 0.3. Furthermore, it is interesting to note that in 26, the filter F1500W is within the region of positive evidence, and reminding the reader that Greene et al. (2023) recently showed that TRAPPIST-1b likely does not have an atmosphere at all, using the F1500W filter.

The result of the second test, changing the semi-major axis, shows the trend of the two-planet model fitting much better as the LTT 1445Ac moves closer to the host star. This makes complete sense, as moving LTT 1445Ac closer will make the planet much hotter and induce a much larger signal. A factor that must be considered is that moving LTT 1445Ac closer also changes the orbital phase, and thus the planet moves much quicker around the star. This means there is an increased chance of a transit/occultation and even a planet-planet occultation in the simulated data. This can be seen in Figure 40 in Appendix 2. Therefore, it is natural that the two-planet model will no doubt be the best fit as these extra occultations and transits would be reproducible with a one-planet model. In the appendix in Figure 44, there can be seen a light curve where LTT 1445Ac is at semi-major axis d = 0.01 AU, where there is no extra transit or occultation induced by LTT 1445Ac, yet the analysis still shows that the two planet model is the best fit. This is due to the significant increase in flux that LTT 1445Ac contributes, as it shows the permanent sub-stellar point. This indicates that if a system has a planet with a very close

orbit, it is easy to distinguish that the secondary planet is present and likely does not have an atmosphere.

Similarly to the phase test, one can look at the filters and their significance in the results. In Figures 27 and 28, it can be seen that for both scatter situations, the 12.8 μm and 15.0 μm filters provide the most significant results. This is due to the error in these filters being relatively low compared to, for example, the 25.5 μm, where there are substantial errors in the simulated data. This was highlighted in Figure 24. This result was surprising to see, as when I created the model light curves in Figure 18, I noticed that it was in this wavelength filter that there was the most significant difference in the flux and that much more signal was being observed. The more significant errors in F2550W are due to this filter's lower throughput, as can be seen in Figure 7. With a lower throughput, this filter is not as efficient at converting the incoming light (photons) into electrons, which gives the signal detected by the instrument, and gives more noise as compared to the other filters.

It is important to note, that specifically for changing the semi-major axis of LTT 1445Ac, the changing of the scatter from being completely different to different for each distance does not change the overall trend of the significance of the filters as the semi-major axis gets smaller and smaller. This can be seen in Figures 27 a) and 28 a). This indicates that the increased signal which is due to the planet getting much warmer, is outweighing the error bars, and thus the model of a two-planet model can only fit the simulated data.

Throughout this thesis, I have shown and talked mainly about the planetary situation of both planets containing no atmosphere. I have also included in my code and my analysis other situations, which include;

- LTT 1445Ac Atmosphere & LTT 1445Ab Atmosphere

- LTT 1445Ac Atmosphere & LTT 1445Ab No atmosphere

- LTT 1445Ac No atmosphere & LTT 1445Ab Atmosphere

As mentioned, the first case, where both planets have an atmosphere, as well as the second case of LTT 1445Ac having an atmosphere, do not give enlightening results, as the effect of LTT 1445Ac with an atmosphere only serves to give an offset or an increase overall of the flux. It is a noticeable effect only when LTT 1445Ac also transits and occults, but if this is not the case, one cannot distinguish through the observed signal if there are two planets or just one. That leaves the last case of LTT 1445Ac with no atmosphere and LTT 1445Ab with an atmosphere. The results mirror the results presented in the results section, and therefore I will not show them in the main body of the thesis, but they will be referenced in Appendix 3.

4.1 Applications

4.1.1 Mini Project

A part of my thesis time while working with the Exoplanet Group at DTU Space, I was asked by my supervisor Lars Buchhave, if I was interested in a mini-project that related to my research. In my presentation of my findings thus far at the time, Lars noticed that I was observing slants in the data where LTT 1445Ac did not have an atmosphere but no slant where LTT 1445Ac did. He had noticed in his data of TRAPPIST-1c from JWST [GO Program 2420] (Rathcke et al., 2021) that there seemed to be a slight slant in the data, and asked me if I could recreate his data with my models. Concretely I was to investigate how an inner planet, TRAPPIST-1b, would affect the signal from TRAPPIST-1c. I set up my code to take in the TRAPPIST-1 system, focusing on two planets, TRAPPIST-1b, and TRAPPIST-1c. In order to recreate the data with my model as best and most accurately as possible, I first set out to calculate the exact position of TRAPPIST-1b when TRAPPIST-1c was transiting. I received the BJD time of TRAPPIST-1c from Lars. I found that TRAPPIST-1b had transited just before TRAPPIST-1c, thus meaning TRAPPIST-1b is moving towards occultation; this gave a phase of 0.82. As in my research for the thesis, I set up the planets with no atmospheres.

Furthermore, I also considered the limb darkening. I calculated the correct limb darkening coefficients for the different wavelengths, such that when I change the wavelength to be observed, the coefficients correspond to the filter. Note, as mentioned earlier, starry at this time is not optimized to include limb darkening for multiple wavelength bins with the spherical harmonic map used to define the primary object (the star). Therefore, I opted to manually change the wavelength for each run, and insert the right limb darkening coefficients for the wavelength when defining the star. I calculated the limb darkening coefficients for four filters, F070W, F090W, F115W and F140M. In Figure 29, I have a visual representation of how the limb darkening coefficients change with wavelengths.

It can be seen in Figure 29 that the limb darkening coefficients change with wavelength significantly, and therefore it shows that this is an important aspect to include, especially when working with transits. With the system set up, the position of TRAPPIST-1b correctly calculated and set, and the limb darkening taken into account, I retrieved the light curves of the system. Figure 30 shows the light curve when TRAPPIST-1b is at phase = 0.82 for the wavelength filter F070W.

Figure 30 indicates that there is no slant induced by TRAPPIST-1b. From my thesis research, this could be due to the orbital phase position of TRAPPIST-1b, as it has most of the
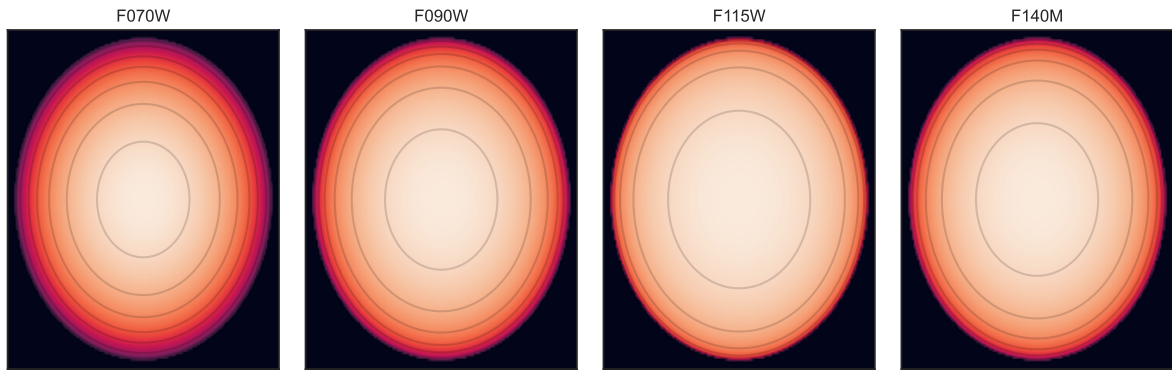
Figure 29: Limb darkening coefficients visualized for the four wavelength filters F070W, F090W, F115W and F140M. As seen, limb darkening depends on the wavelength, as we see the varying degree of the effect for each wavelength.
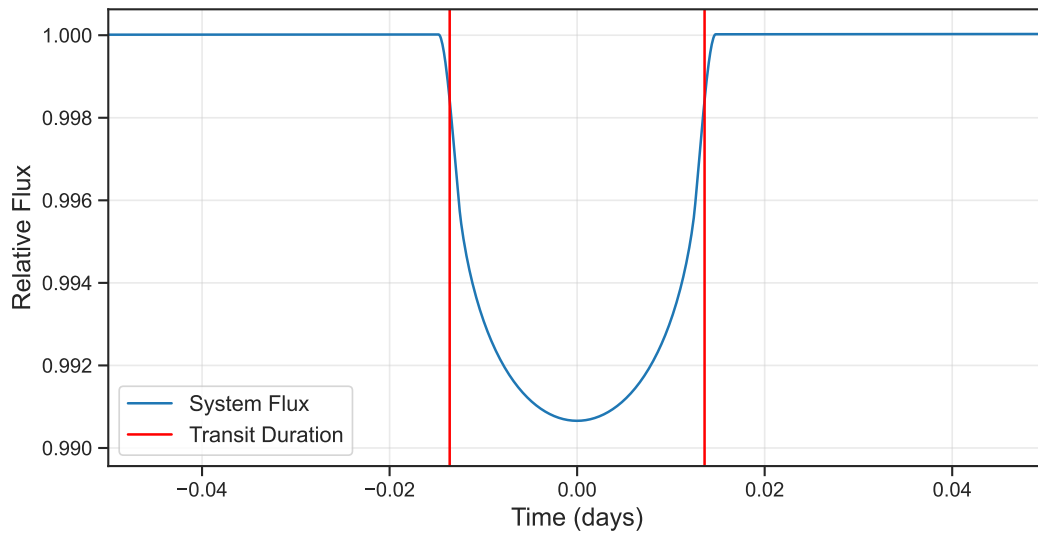

Figure 30: The light curve of the TRAPPIST-1 system, including only planets TRAPPIST-1b and TRAPPIST-1c, using the F070W filter. We are observing the transit of TRAPPIST-1c and have calculated where TRAPPIST-1b is when TRAPPIST-1c transits, resulting in a phase of 0.82. We see here that there is no observed slant with the model, indicating that TRAPPIST-1b is not noticeable in the data. This means that the slant observed by Lars in his data is most likely due to other effects.

"night-side" facing the observer and thus does not induce a significant effect on the observed flux. The slant that is observed in Lars' data is most likely due to other factors and not a sign of TRAPPIST-1b.

4.1.2 Flux Calibration

When creating my light curves and seeing the results, I noticed that when we have the unscaled data, see Figure 22, there is a significant difference in the flux of the two models (Two-planet vs. one-planet model). This led me to think, if there was a way to know or estimate the flux one would expect from a system that, upon further knowledge, only includes a single

planet, could an observation that mirrors Figure 22, not give insight that there is a secondary planet somewhere in the system. My models and simulated data are only relative fluxes. Thus in my situation, this can not be implemented, and therefore I needed to scale the one-planet model and simulated data. If observations that are not relative fluxes are made, this could be a real method to distinguish what is seen in the signal. Albeit, this is a theoretical idea, as this has not been explored yet. However, with the stability of JWST over a time series, this could be a potential new method to detect other planets in systems.

5 Conclusion

This thesis sought to investigate the possible effects a planetary sibling could induce on the measured light curve of a target planet in occultation. Specifically, this thesis looked at the exoplanet system of LTT 1445A, a system of two planets orbiting an M-dwarf star. This system was chosen due to the proximity of the system and the nature of the host star. The thesis aimed to simulate JWST data and perform tests to probe whether specific configurations of the system have significant impacts on the observed signal, leading to the characterization of a sibling planet. Concretely, I investigated whether the planetary sibling LTT 1445Ac significantly affected the observation of LTT 1445Ab (the target planet) in secondary eclipse. Through the simulated data and statistical analysis with models, I conclude that specific configurations significantly favor a two-planet model with no atmosphere over the single-planet model. These configurations include the orbital phase of LTT 1445Ac at phases 0.3 and 0.7 for wavelengths 12.8, 15.0, and 21.0 μm. The results further show, that when astronomers seek to distinguish if planets have atmospheres or not, they must take into account the configuration of the system, in order to get the best results.

Terrestrial planets are the frequent targets of JWST cycle 1 & 2, with several programs dedicated to them, such as Rathcke et al. (2021) [GO 2420] from cycle 1, and [GO 3730] from cycle 2 [8]. Specifically, the program GO 3730 from cycle 2 (a program in which I am a co-investigator) will investigate the presence of atmospheres of terrestrial worlds in secondary eclipse and use many of the same methods as explored in this thesis. With the results presented in this thesis, and the aim of GO 3730, this program is projected to be exciting, and the chances of characterizing more terrestrial exoplanets are hopeful.

---

[8]GO 3730 Program Information - STScI

References

Berta-Thompson, Z. K., Diamond-Lowe, H., & Winters, J. 2021, The Thermal Emission Spectrum of the Closest M Dwarf Transiting Rocky Planet, JWST Proposal. Cycle 1, ID. #2708

Borucki, W. J., et al. 2010, Kepler Planet-Detection Mission: Introduction and First Results, Science, 327, 977

Bradt, H. 2003, Detectors and statistics (Cambridge University Press), 130–174

Brown, T. M., Charbonneau, D., Gilliland, R. L., Noyes, R. W., & Burrows, A. 2001, Hubble Space Telescope Time-Series Photometry of the Transiting Planet of HD 209458, ApJ, 552, 699

Carroll, B. W., & Ostlie, D. A. 2017, An introduction to modern astrophysics, Second Edition

Charbonneau, D., Brown, T. M., Latham, D. W., & Mayor, M. 2000, Detection of Planetary Transits Across a Sun-like Star, ApJ, 529, L45

Charbonneau, D., Brown, T. M., Noyes, R. W., & Gilliland, R. L. 2002, Detection of an Extrasolar Planet Atmosphere, ApJ, 568, 377

Deming, D., et al. 2013, Infrared Transmission Spectroscopy of the Exoplanets HD 209458b and XO-1b Using the Wide Field Camera-3 on the Hubble Space Telescope, ApJ, 774, 95

Dressing, C. D., & Charbonneau, D. 2013, The Occurrence Rate of Small Planets around Small Stars, ApJ, 767, 95

—. 2015, The Occurrence of Potentially Habitable Planets Orbiting M Dwarfs Estimated from the Full Kepler Dataset and an Empirical Measurement of the Detection Sensitivity, ApJ, 807, 45

Greene, T. P., Bell, T. J., Ducrot, E., Dyrek, A., Lagage, P.-O., & Fortney, J. J. 2023, Thermal emission from the Earth-sized exoplanet TRAPPIST-1 b using JWST, arXiv e-prints, arXiv:2303.14849

JWST User Documentation. 2016, JWST User Documentation (JDox), JWST User Documentation Website

Kanodia, S., et al. 2023, TOI-5205b: A Short-period Jovian Planet Transiting a Mid-M Dwarf, AJ, 165, 120

Koll, D. D. B., Malik, M., Mansfield, M., Kempton, E. M. R., Kite, E., Abbot, D., & Bean, J. L. 2019, Identifying Candidate Atmospheres on Rocky M Dwarf Planets via Eclipse Photometry, ApJ, 886, 140

Kreidberg, L., et al. 2014, Clouds in the atmosphere of the super-Earth exoplanet GJ1214b, Nature, 505, 69

—. 2019, Absence of a thick atmosphere on the terrestrial exoplanet LHS 3844b, Nature, 573, 87

Latham, D. W., Mazeh, T., Stefanik, R. P., Mayor, M., & Burki, G. 1989, The unseen companion of HD114762: a probable brown dwarf, Nature, 339, 38

Lorah, J., & Womack, A. 2019, Value of sample size for computation of the Bayesian information criterion (BIC) in multilevel modeling, Behavior research methods, 51, 440

Lovis, C., & Fischer, D. 2010, in Exoplanets, ed. S. Seager, 27–53

Luger, R., Agol, E., Foreman-Mackey, D., Fleming, D. P., Lustig-Yaeger, J., & Deitrick, R. 2019, starry: Analytic Occultation Light Curves, AJ, 157, 64

Mayor, M., & Queloz, D. 1995, A Jupiter-mass companion to a solar-type star, Nature, 378, 355

Moran, S. E., et al. 2023, High Tide or Riptide on the Cosmic Shoreline? A Water-Rich Atmosphere or Stellar Contamination for the Warm Super-Earth GJ~486b from JWST Observations, arXiv e-prints, arXiv:2305.00868

NASA Exoplanet Archive. 2023, Planetary Systems

NASA Historic Timeline. 2022, Historic timeline

Rathcke, A., et al. 2021, Probing the Terrestrial Planet TRAPPIST-1c for the Presence of an Atmosphere, JWST Proposal. Cycle 1, ID. #2420

Rauscher, B. J., & Ressler, M. E. 2005, The James Webb Space Telescope and its Infrared Detectors, Experimental Astronomy, 19, 149

Schwarz, G. 1978, Estimating the Dimension of a Model, Annals of Statistics, 6, 461

Seager, S., & Deming, D. 2009, On the Method to Infer an Atmosphere on a Tidally Locked Super Earth Exoplanet and Upper Limits to GJ 876d, ApJ, 703, 1884

Seager, S., & Lissauer, J. J. 2010, in Exoplanets, ed. S. Seager, 3–13

Segura, A., Kasting, J. F., Meadows, V., Cohen, M., Scalo, J., Crisp, D., Butler, R. A. H., & Tinetti, G. 2005, Biosignatures from Earth-Like Planets Around M Dwarfs, Astrobiology, 5, 706

Sing, D. K., et al. 2016, A continuum from clear to cloudy hot-Jupiter exoplanets without primordial water depletion, Nature, 529, 59

Smith, A. M. S., et al. 2018, K2-137 b: an Earth-sized planet in a 4.3-h orbit around an M-dwarf, MNRAS, 474, 5523

Smith, B. A., & Terrile, R. J. 1984, A Circumstellar Disk around β Pictoris, Science, 226, 1421

Winn, J. N. 2010, in Exoplanets, ed. S. Seager, 55–77

Winters, J. G., et al. 2019, Three Red Suns in the Sky: A Transiting, Terrestrial Planet in a Triple M-dwarf System at 6.9 pc, AJ, 158, 152

—. 2022, A Second Planet Transiting LTT 1445A and a Determination of the Masses of Both Worlds, AJ, 163, 168

Wolszczan, A., & Frail, D. A. 1992, A planetary system around the millisecond pulsar PSR1257 + 12, Nature, 355, 145
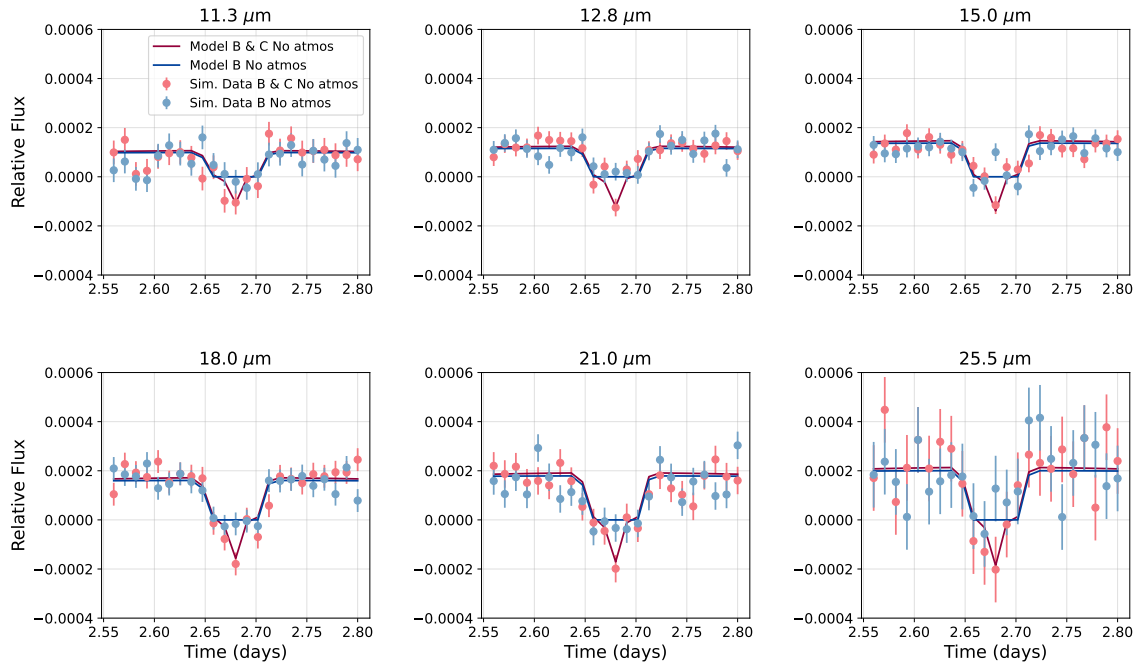
6 Appendix 1: Light Curves for Phase Changes
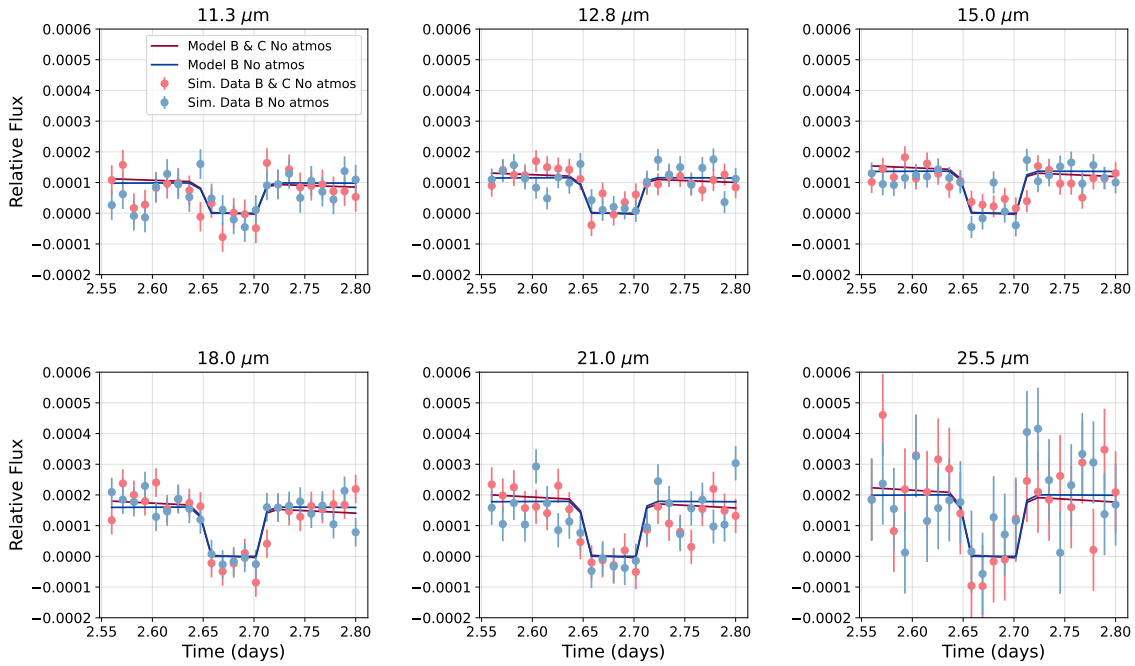
Figure 31: Light Curves at different wavelengths for LTT 1445Ac at phase = 0.25, when LTT 1445Ab is at phase = 0.5 (the midpoint of occultation). For system set up: LTT 1445Ab with no atmosphere, LTT 1445Ac with no atmosphere
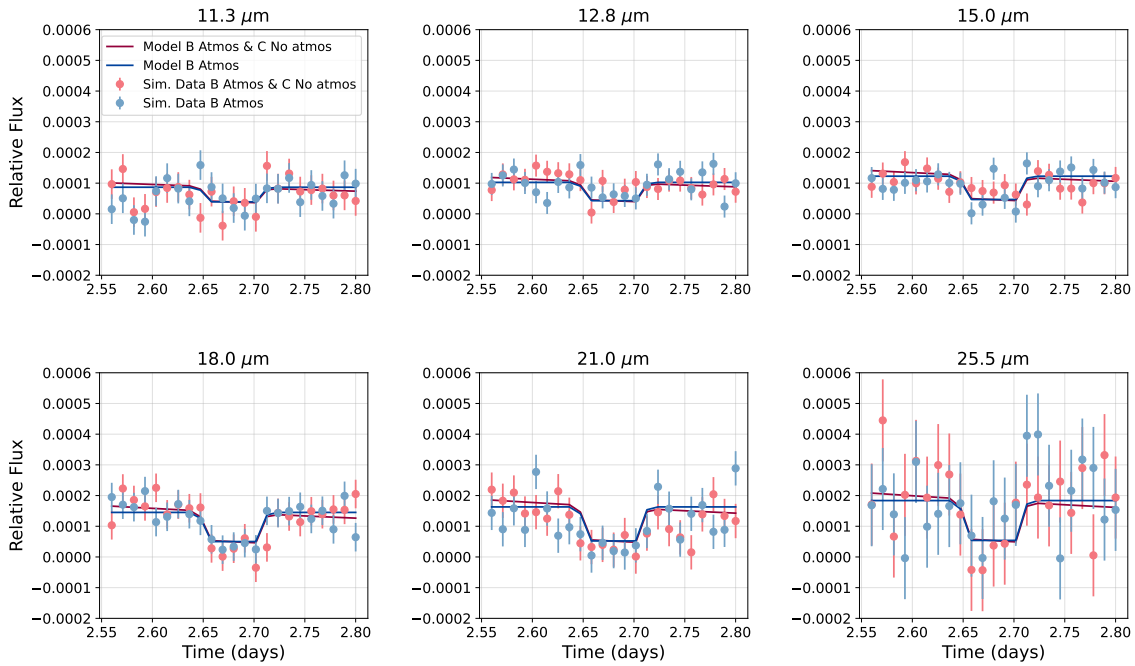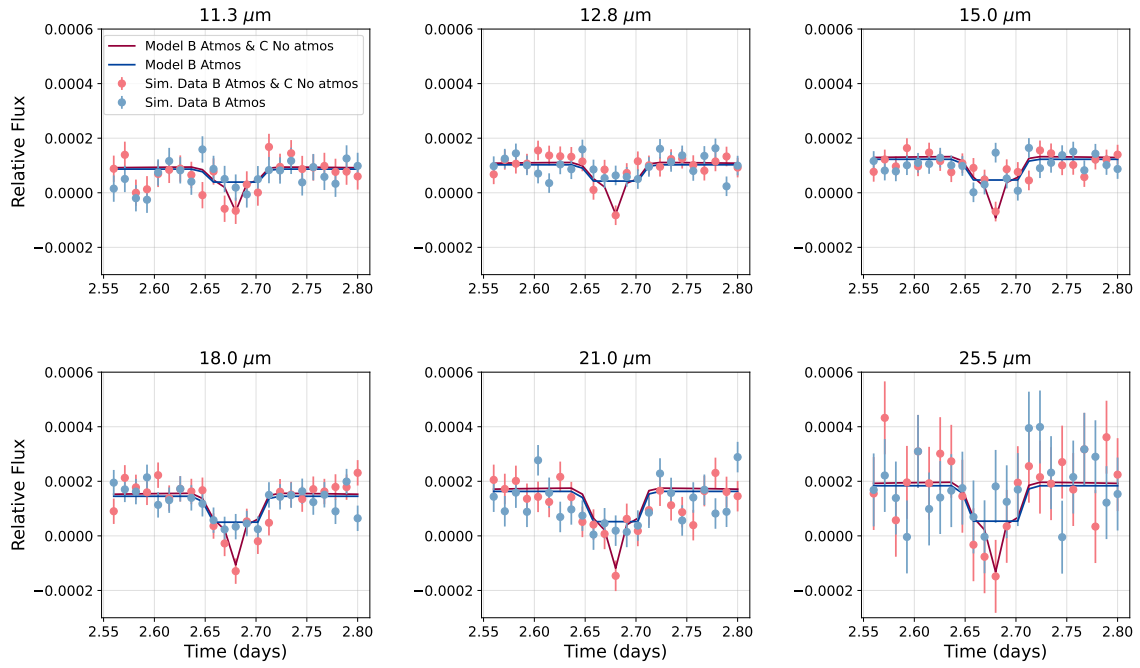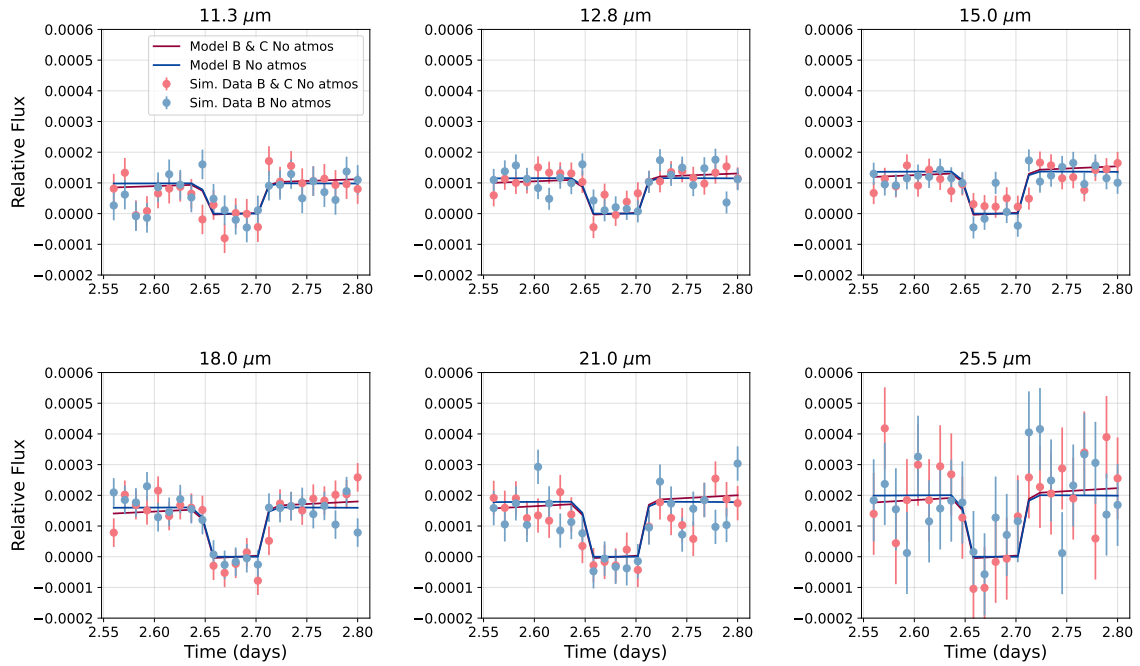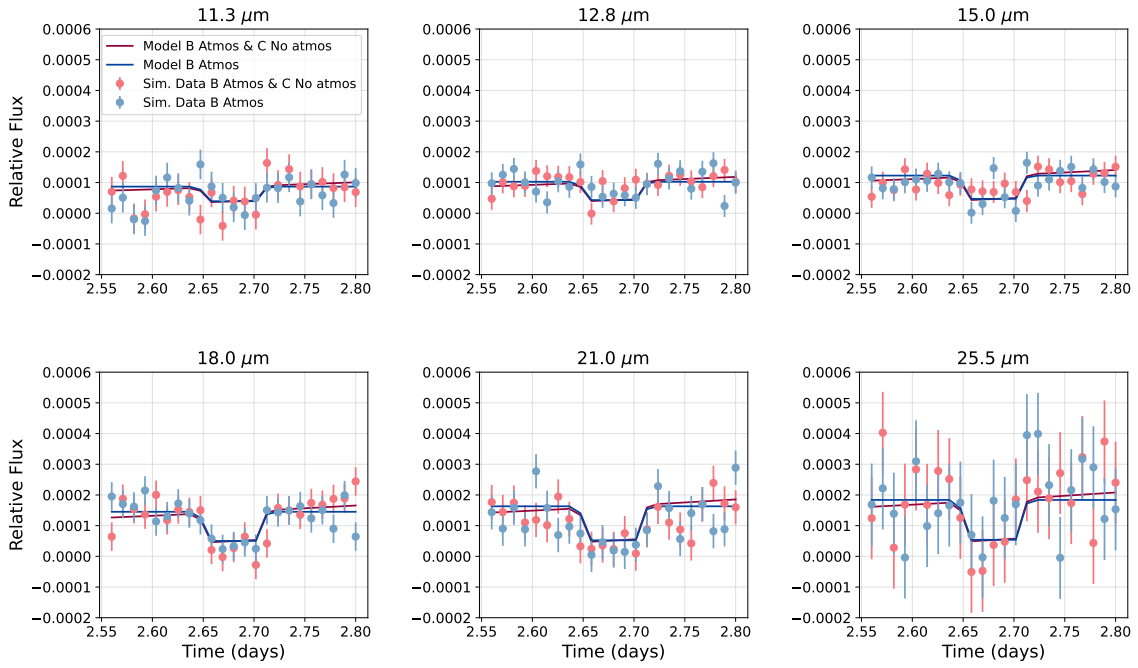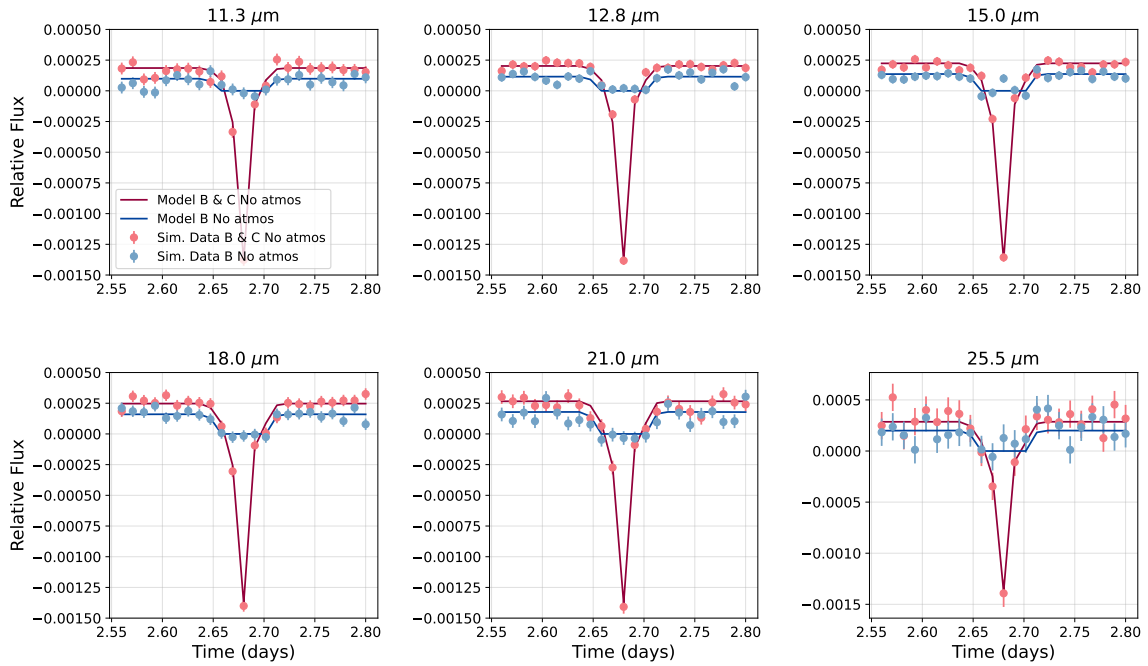

Figure 32: Light Curves at different wavelengths for LTT 1445Ac at phase = 0.25, when LTT 1445Ab is at phase = 0.5 (the midpoint of occultation). For system set up: LTT 1445Ab with an atmosphere, LTT 1445Ac with no atmosphere
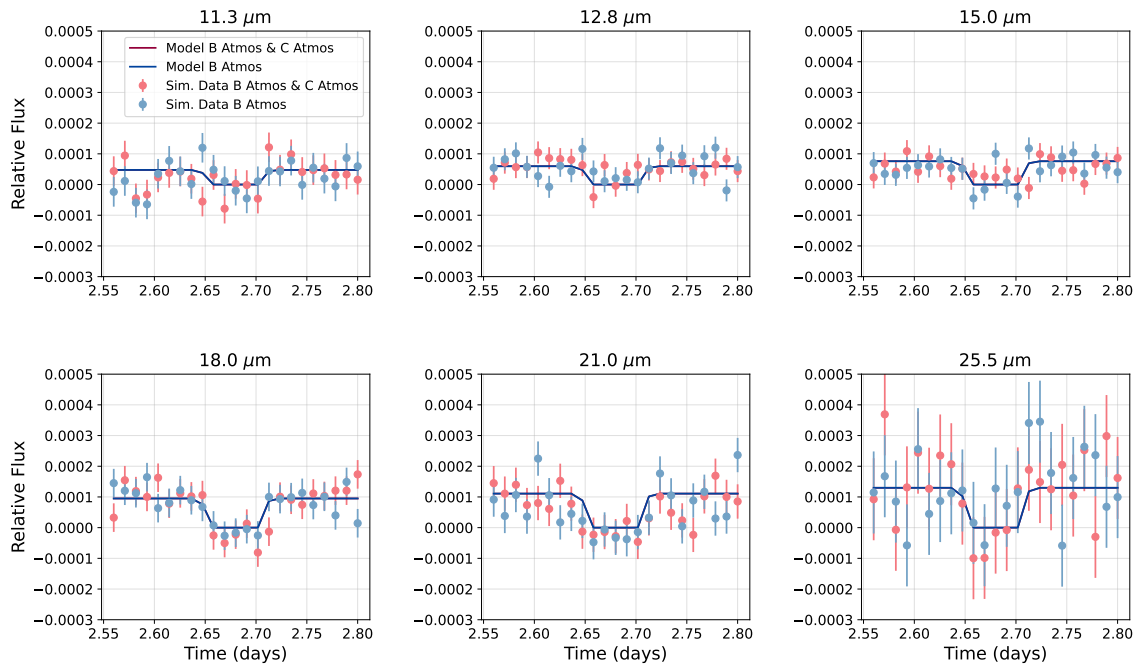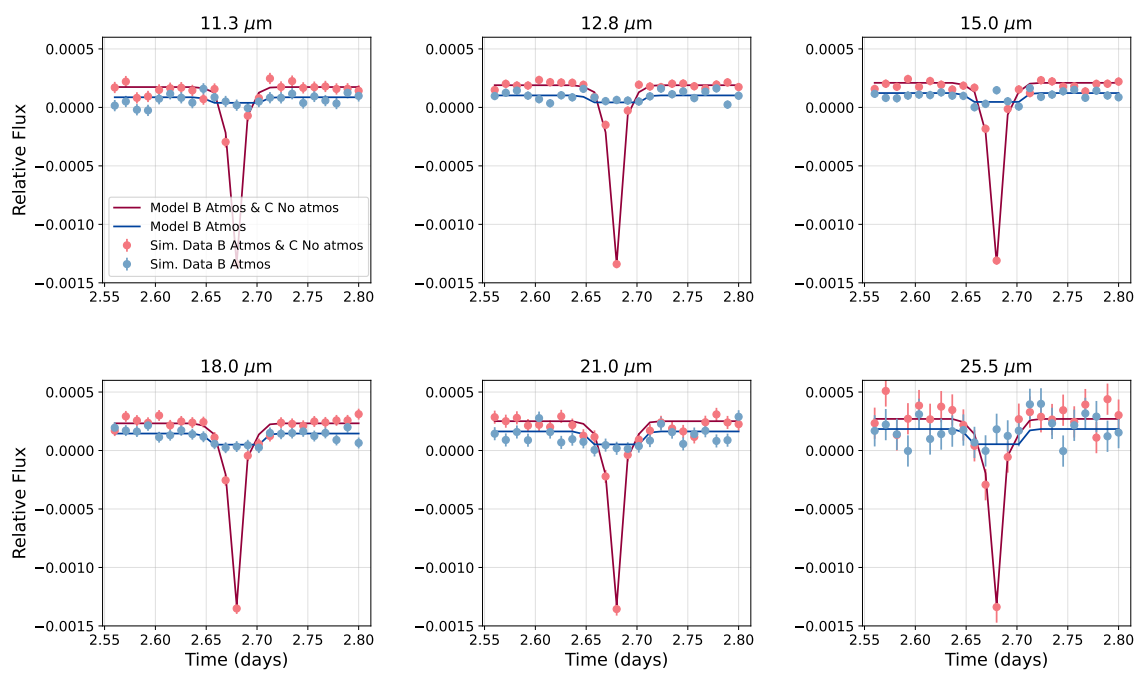
Figure 33: Light Curves at different wavelengths for LTT 1445Ac at phase = 0.25, when LTT 1445Ab is at phase = 0.5 (the midpoint of occultation). For system set up: LTT 1445Ab with an atmosphere, LTT 1445Ac with an atmosphere

Figure 34: Light Curves at different wavelengths for LTT 1445Ac at phase = 0.5, when LTT 1445Ab is at phase = 0.5 (the midpoint of occultation). For system set up: LTT 1445Ab with no atmosphere, LTT 1445Ac with no atmosphere

Figure 35: Light Curves at different wavelengths for LTT 1445Ac at phase = 0.5, when LTT 1445Ab is at phase = 0.5 (the midpoint of occultation). For system set up: LTT 1445Ab with an atmosphere, LTT 1445Ac with no atmosphere

Figure 36: Light Curves at different wavelengths for LTT 1445Ac at phase = 0.75, when LTT 1445Ab is at phase = 0.5 (the midpoint of occultation). For system set up: LTT 1445Ab with no atmosphere, LTT 1445Ac with no atmosphere

Figure 37: Light Curves at different wavelengths for LTT 1445Ac at phase = 0.75, when LTT 1445Ab is at phase = 0.5 (the midpoint of occultation). For system set up: LTT 1445Ab with an atmosphere, LTT 1445Ac with no atmosphere

Figure 38: Light Curves at different wavelengths for LTT 1445Ac at phase = 1, when LTT 1445Ab is at phase = 0.5 (the midpoint of occultation). For system set up: LTT 1445Ab with no atmosphere, LTT 1445Ac with no atmosphere

Figure 39: Light Curves at different wavelengths for LTT 1445Ac at phase = 1, when LTT 1445Ab is at phase = 0.5 (the midpoint of occultation). For system set up: LTT 1445Ab with an atmosphere, LTT 1445Ac with no atmosphere
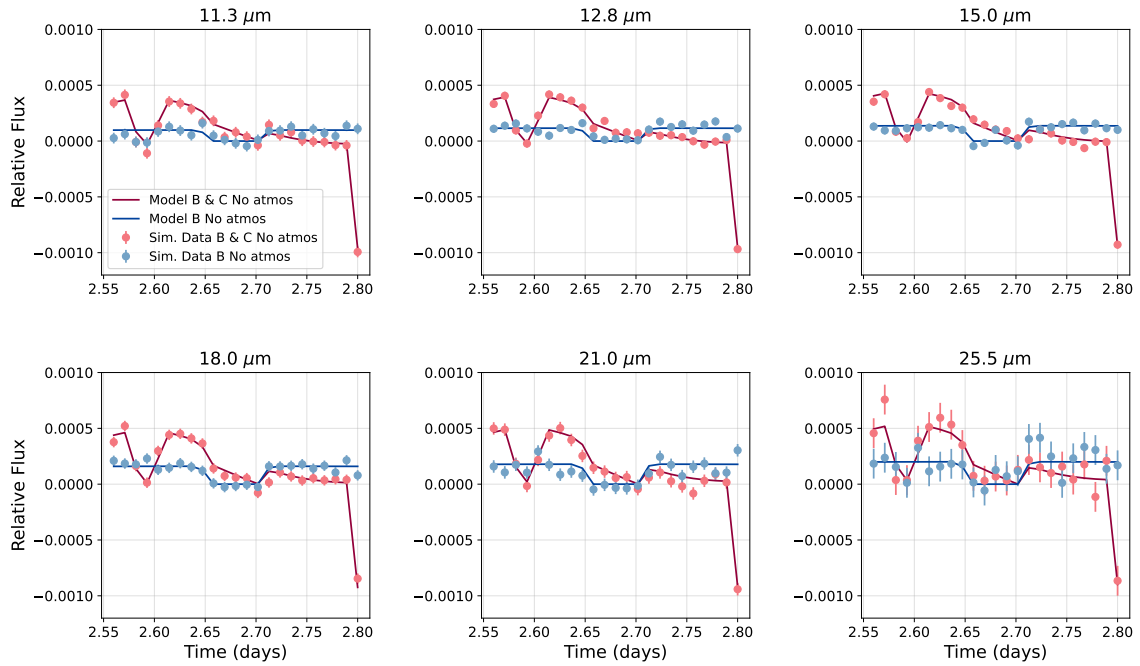
7 Appendix 2: Light Curves for Semi Major Axis Changes
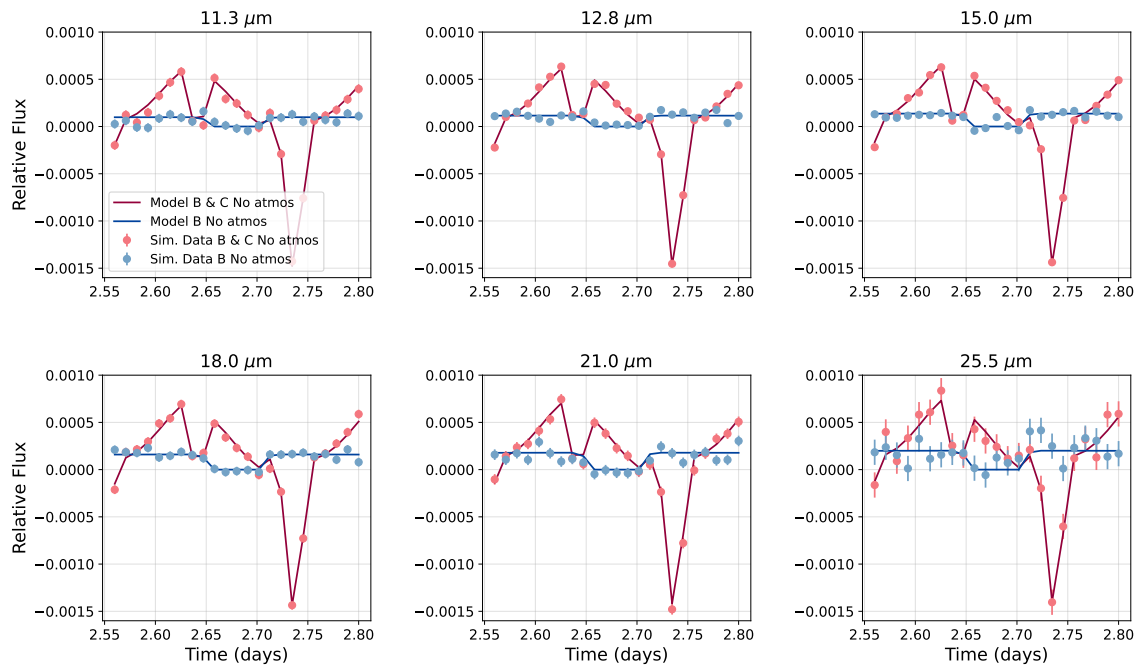
Figure 40: Light Curves at different wavelengths for semi-major axis of LTT 1445Ac, d = 0.004 AU and LTT 1445Ac at phase = 0.3, when LTT 1445Ab is at phase = 0.5, and distance kept at the correct value. For system set up: B with n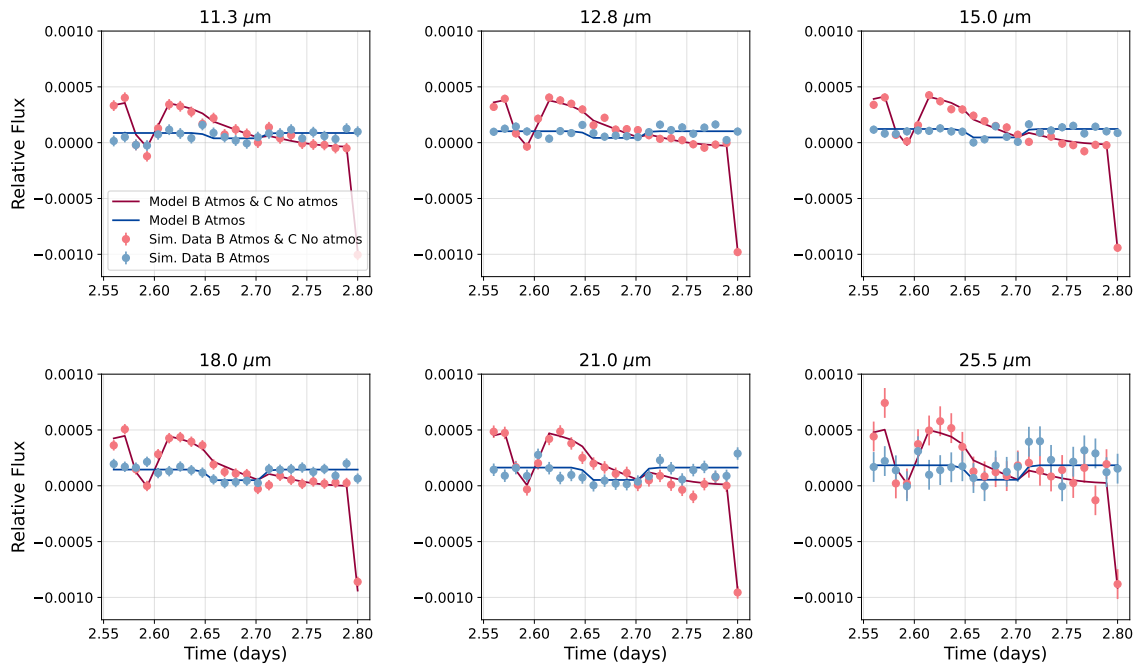o atmosphere, C with no atmosphere. We see the effect of LTT 1445Ac containing a very hot dayside, as the planet is very close to the host star. Furthermore, we also see a transit coupled with a planet-planet occultation (where the LTT 1445Ac moves in front of LTT 1445Ab), due to the very short orbit of LTT 1445Ac.
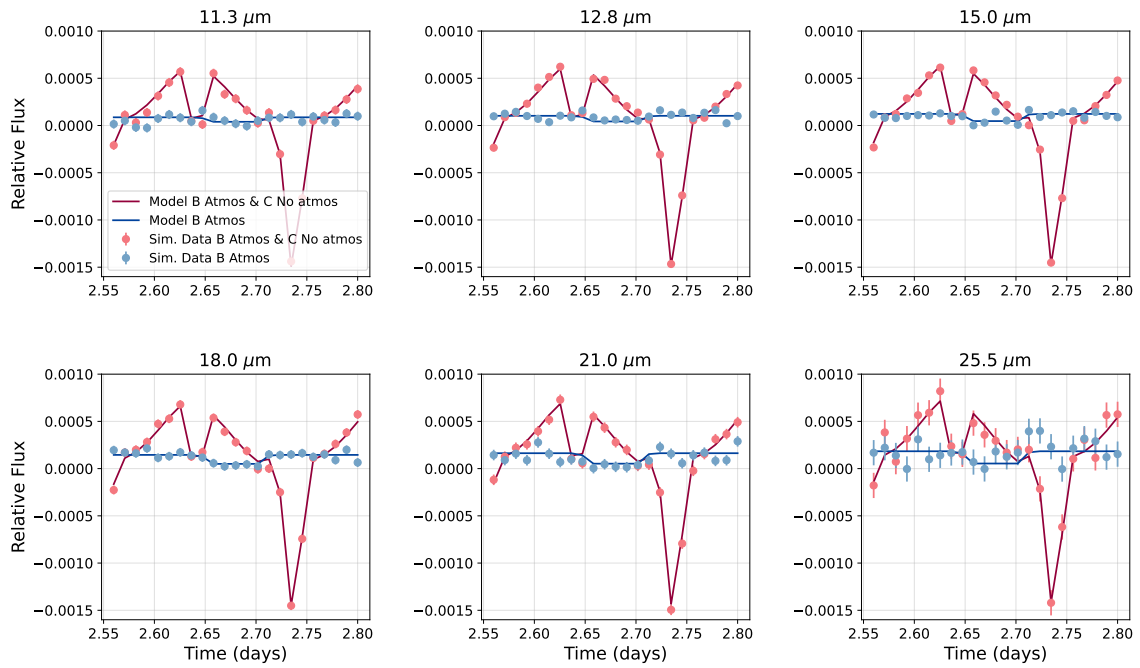
Figure 41: Light Curves at different wavelengths for semi-major axis of LTT 1445Ac, d = 0.004 AU and LTT 1445Ac at phase = 0.3, when LTT 1445Ab is at phase = 0.5, and distance kept at the correct value. For system set up: B with an atmosphere, C with no atmosphere.
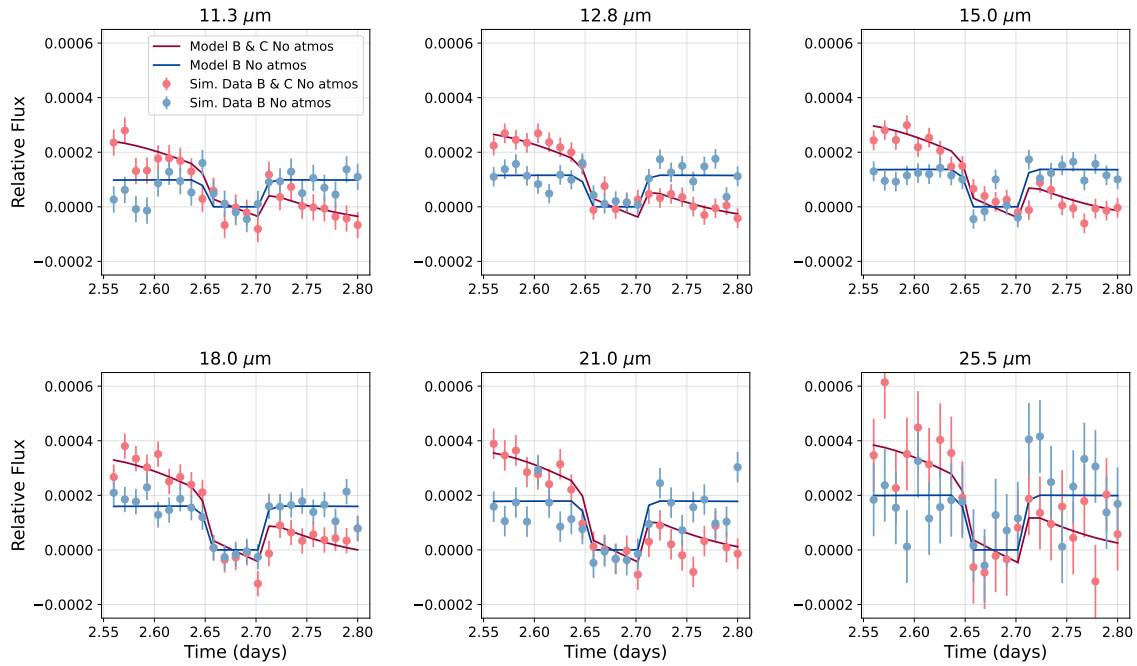

Figure 42: Light Curves at different wavelengths for semi-major axis of LTT 1445Ac, d = 0.007 AU and LTT 1445Ac at phase = 0.3, when LTT 1445Ab is at phase = 0.5, and distance kept at the correct value. For system set up: B with no atmosphere, C with no atmosphere.
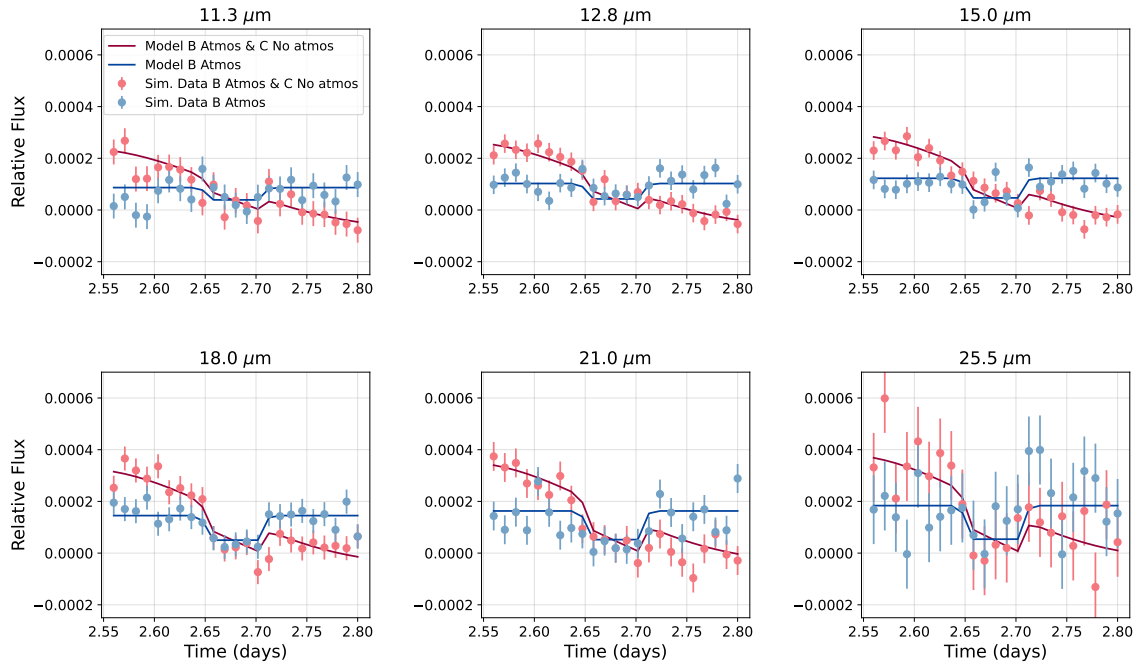
Figure 43: Light Curves at different wavelengths for semi-major axis of LTT 1445Ac, d = 0.007 AU and LTT 1445Ac at phase = 0.3, when LTT 1445Ab is at phase = 0.5, and distance kept at the correct value. For system set up: B with an atmosphere, C with no atmosphere.

Figure 44: Light Curves at different wavelengths for semi-major axis of LTT 1445Ac, d = 0.01 AU and LTT 1445Ac at phase = 0.3, when LTT 1445Ab is at phase = 0.5, and distance kept at the correct value. For system set up: B with no atmosphere, C with no atmosphere.
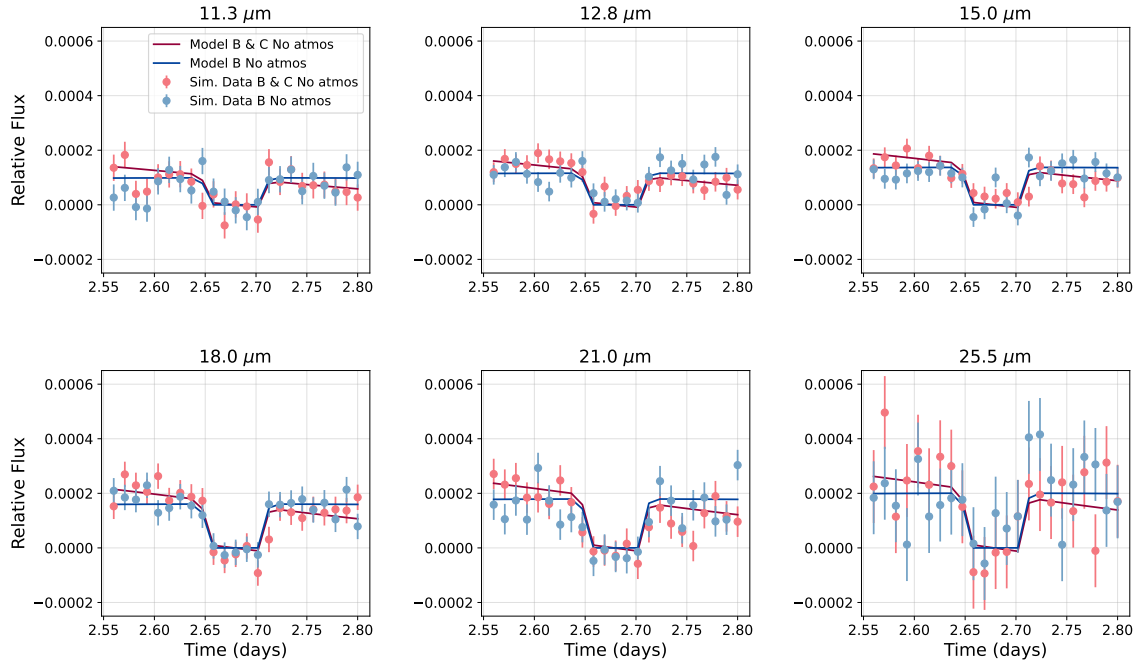
Figure 45: Light Curves at different wavelengths for semi-major axis of LTT 1445Ac, d = 0.01 AU and LTT 1445Ac at phase = 0.3, when LTT 1445Ab is at phase = 0.5, and distance kept at the correct value. For system set up: B with an atmosphere, C with no atmosphere.
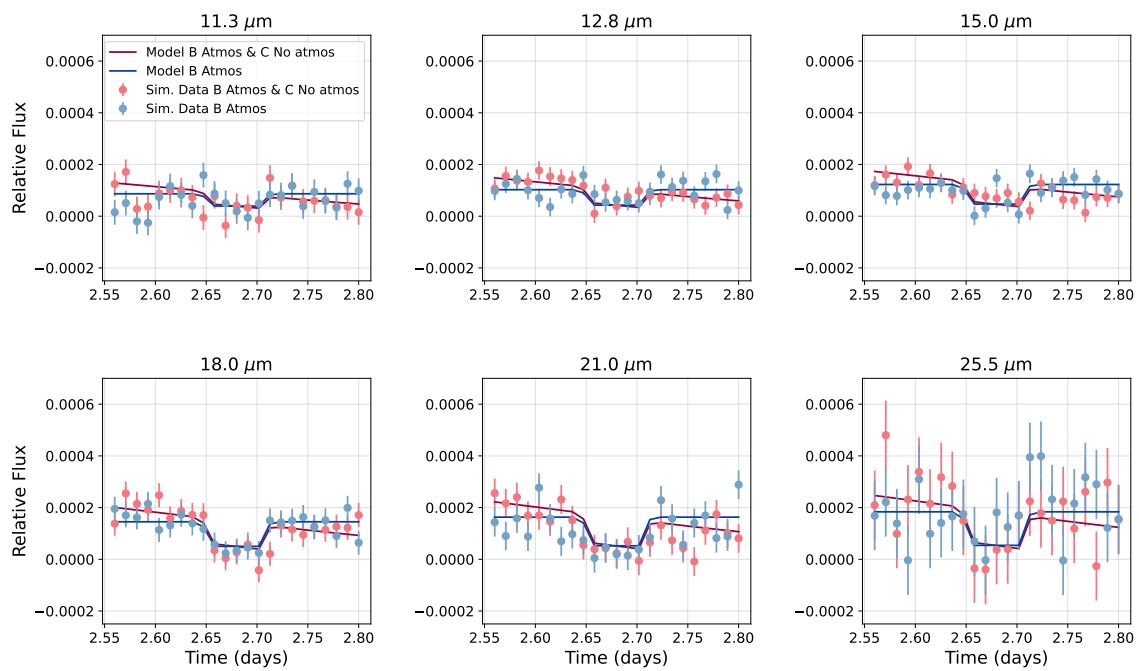

Figure 46: Light Curves at different wavelengths for semi-major axis of LTT 1445Ac, d = 0.018 AU and LTT 1445Ac at phase = 0.3, when LTT 1445Ab is at phase = 0.5, and distance kept at the correct value. For system set up: B with no atmosphere, C with no atmosphere.

Figure 47: Light Curves at different wavelengths for semi-major axis of LTT 1445Ac, d = 0.018 AU and LTT 1445Ac at phase = 0.3, when LTT 1445Ab is at phase = 0.5, and distance kept at the correct value. For system set up: B with an atmosphere, C with no atmosphere.
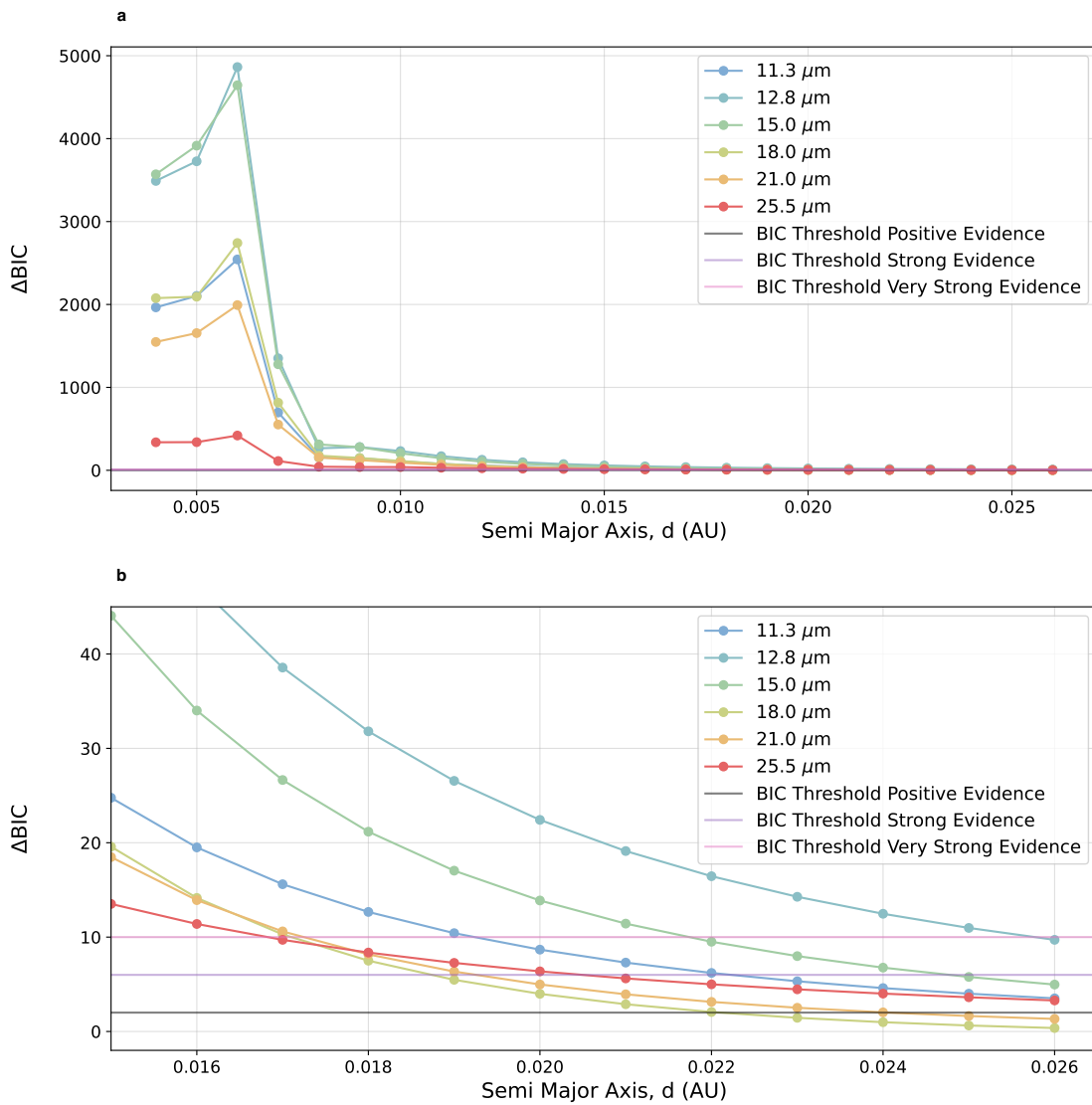
8 Appendix 3: Extra BIC plots

Figure 48: BIC Difference Plot for LTT 1445Ac (phase = 0.3). System set up: LTT 1445Ac No atmosphere, LTT 1445Ab Atmosphere.
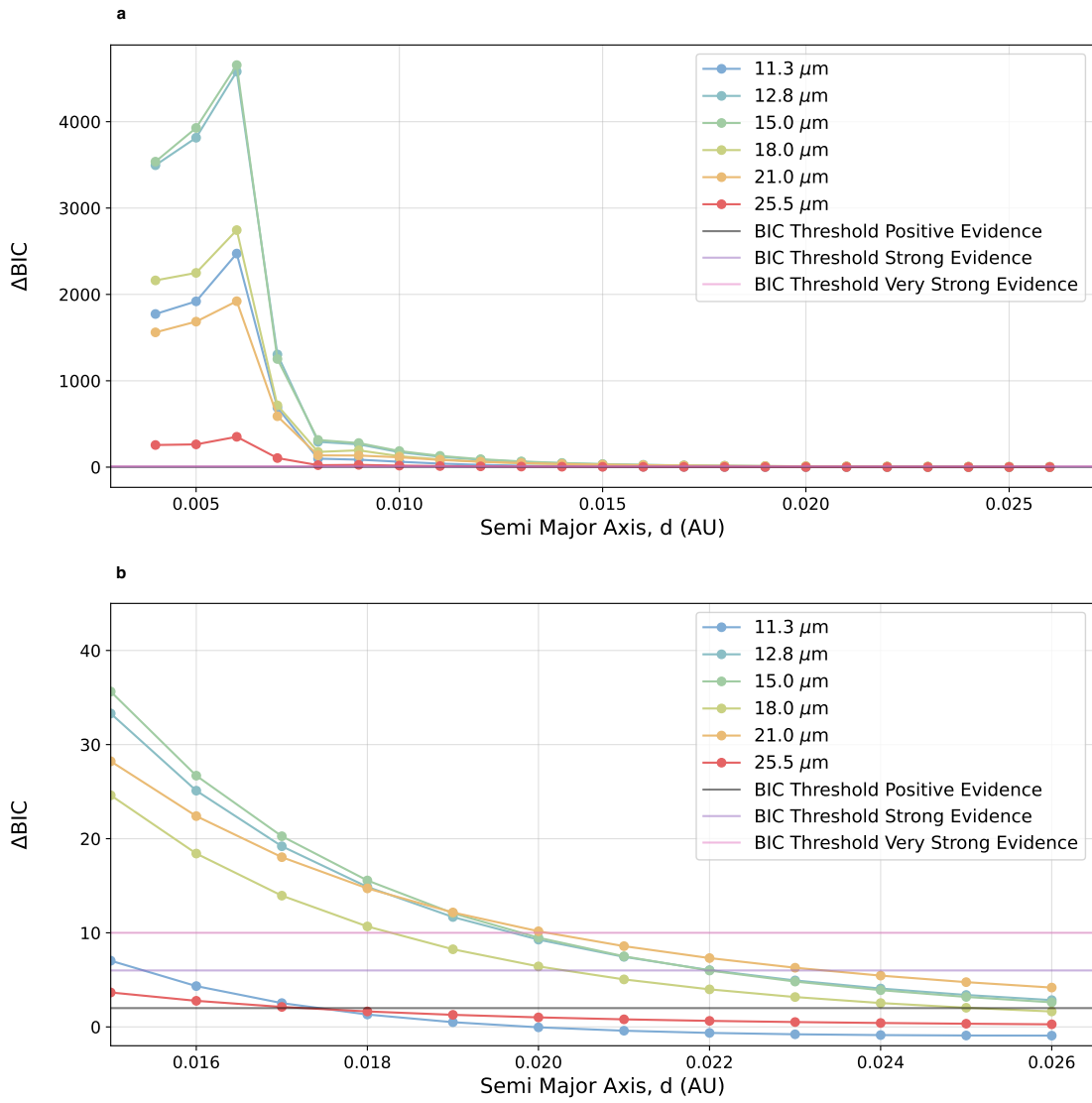
Figure 49: BIC Difference Plot for LTT 1445Ac No atmosphere, LTT 1445Ab Atmosphere situation